Published in final edited form as:

Mol Cell. 2022 December 15; 82(24): 4627–4646.e14. doi:10.1016/j.molcel.2022.11.002.

Tip60-mediated H2A.Z acetylation promotes neuronal fate specification and bivalent gene activation

Justyna A. Janas[1,2,3], **Lichao Zhang**[3], **Jacklyn H. Luu**[1,2,3], **Janos Demeter**[4], **Lingjun Meng**[1,2,3], **Samuele G. Marro**[1,2,3,6,7], **Moritz Mall**[1,2,3,8], **Nancie A. Mooney**[4], **Katie Schaukowitch**[1,2,3], **Yi Han Ng**[1,2,3], **Nan Yang**[1,2,3,6,7], **Yuhao Huang**[1,2,3], **Gernot Neumayer**[1,2,3], **Or Gozani**[5], **Joshua E. Elias**[3,9], **Peter K. Jackson**[1,4], **Marius Wernig**[1,2,3,*]

[1]Department of Pathology, Stanford University School of Medicine, Stanford, CA 94305, USA.

[2]Institute for Stem Cell Biology and Regenerative Medicine, Stanford University School of Medicine, Stanford, CA 94305, USA.

[3]Department of Chemical and Systems Biology, Stanford University School of Medicine, Stanford, CA 94305, USA.

[4]Baxter Laboratory, Department of Microbiology & Immunology, Stanford University School of Medicine, Stanford, CA 94305, USA.

[5]Department of Biology, Stanford University, Stanford, CA 94305, USA.

[6]Present address: Black Family Stem Cell Institute, Icahn School of Medicine at Mount Sinai, New York, NY 10029, USA.

[7]Present address: Nash Family Department of Neuroscience, Friedman Brain Institute, Icahn School of Medicine at Mount Sinai, New York, NY 10029, USA.

[8]Present address: Cell Fate Engineering and Disease Modeling Group, German Cancer Research Center (DKFZ) and DKFZ-ZMBH Alliance; Hector Institute for Translational Brain Research gGmbH, 69120, Heidelberg, Germany; Central Institute of Mental Health, Medical Faculty Mannheim, Heidelberg University, 68159, Mannheim, Germany.

[9]Present address: Mass Spectrometry Platform, Chan Zuckerberg Biohub; Stanford, USA.

Summary

[*]Lead Contact: wernig@stanford.edu.

Author contributions

J.A.J. and M.W. conceived and designed the study. J.A.J. performed the experiments and data analyses. L.Z. performed mass spectrometry experiments. J.D., L.Z. and J.A.J. analyzed proteomics data. J.H.L. and J.A.J. performed image analysis. J.H.L., Y.H. assisted in knockdown experiments. S.G.M. and J.A.J. designed *Kat5* cKO targeting strategy. L.M. and J.A.J. generated Tip60 cKO mouse. M.M. and N.A.M. performed BioID and LAP pulldowns. KS performed FRAP experiments. Y.H.N. generated inducible mES line. N.Y. and J.A.J. optimized Cut&Tag. G.N. provided TIP60 plasmid. O.G., P.K.J. and J.E.E. provided critical advice on experimental design and data interpretation. J.A.J. and M.W. wrote the manuscript.

Declaration of Interests

The authors declare no competing interests.

Cell lineage specification is accomplished by a concerted action of chromatin remodeling and tissue-specific transcription factors. However, the mechanisms that induce and maintain appropriate lineage-specific gene expression remain elusive. Here, we used an unbiased proteomics approach to characterize chromatin regulators that mediate the induction of neuronal cell fate. We found that Tip60 acetyltransferase is essential to establish neuronal cell identity partly via acetylation of the histone variant H2A.Z. Despite its tight correlation with gene expression and active chromatin, loss of H2A.Z acetylation had little effect on chromatin accessibility or transcription. Instead, loss of Tip60 and acetyl-H2A.Z interfered with H3K4me3 deposition and activation of a unique subset of silent, lineage-restricted genes characterized by a bivalent chromatin configuration at their promoters. Altogether, our results illuminate the mechanisms underlying bivalent chromatin activation and reveal that H2A.Z acetylation regulates neuronal fate specification by establishing epigenetic competence for bivalent gene activation and cell lineage transition.

Graphical Abstract

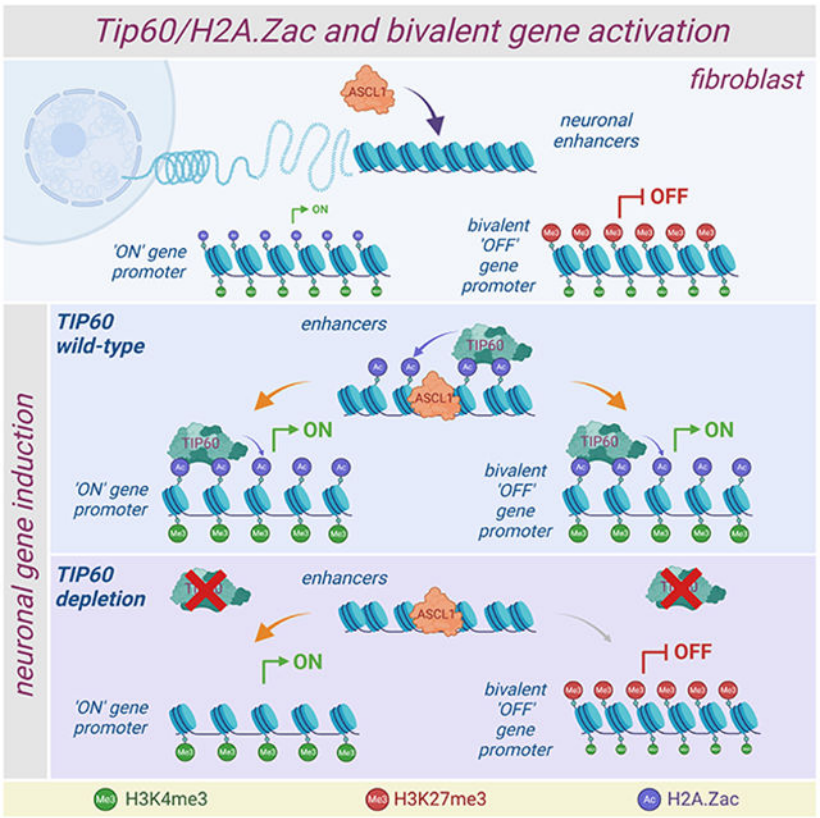

eTOC Blurb

Janas et al. report that Tip60 acetyltransferase is essential for neuronal cell fate specification. The study reveals that one of the functions of Tip60 during neuronal induction is the acetylation of histone variant H2A.Z, which promotes H3K4me3 deposition and bivalent gene activation, thus establishing epigenetic competence for cell lineage transition.

Keywords

Tip60/Kat5; Ascl1; H2A.Z acetylation; cell fate; neurogenesis; transcription; bivalent chromatin; gene activation; H3K4me3

Introduction

The emergence of new cell fates during development results from dynamic gene expression changes driven by a complex interaction of tissue-specific transcription factors (TFs) with the chromatin and chromatin regulators. The instructive role of TFs in establishing new transcription and epigenetic programs has been emphasized by reprogramming experiments, such as induction of pluripotent stem cells, neurons, hepatocytes, hematopoietic cells and others, from non-related cells upon the expression of TFs[1]. While alone not instructive, chromatin modulating factors are essential to facilitate and enable the transcriptional output of TF-chromatin binding events[2-5]. It is chromatin factors that create the fluidity and complexity of the chromatin, which greatly influences TF recruitment and site-specific activity of the transcriptional machinery[6].

With regards to neuronal cell fate specification many classes of TFs have been investigated in detail[7,8]. Among them proneuronal basic helix–loop–helix (bHLH) TFs have emerged as most prominent and powerful neuronal inducers. Proneuronal bHLH factors, such as Neurogenin2 (Ngn2) and Ascl1, oppose the effects of the Notch pathway and its downstream HLH factors, like Hes1 and Hes5, and induce the differentiation of dividing ventricular zone (VZ) neural progenitor cells (NPCs) by activating the neuronal transcription program[9-12]. Intriguingly, the Notch/proneural factor balance is accomplished through oscillation of Hes1 in VZ progenitors, which inhibits Ascl1 by triggering its anti-phasic expression and thus creating a poised state for differentiation[13]. Accordingly, bHLH factors like Ascl1 are so potent that they can induce functional neurons (so-called induced neuronal (iN) cells) from unrelated lineages, such as fibroblasts[14,15]. In this context, Ascl1 acts on the top of a hierarchical mechanism as an ‘on target’ pioneer factor that binds to its physiological target sites on closed chromatin initiating rapid local and genome-wide chromatin changes[16,17]. However, how the proneural bHLH factors initiate chromatin changes that ultimately lead to the activation of the neuronal transcription program and cell identity, remains unclear.

Nucleosomes are central to chromatin-TF interactions that allow for cell-type specific gene regulation. Much of their functional diversity is conferred by histone variants and their dynamic regulation by post-translational modifications (PTMs). The histone variant H2A.Z emerged as essential for lineage commitment by playing many diverse and often opposing functions in gene regulation[18,19]. The contrasting roles of H2A.Z are attributed to its modulation by PTMs. As such, for instance, acetylation of H2A.Z (H2A.Zac) was shown to correlate with active transcription, whereas its ubiquitination is thought to associate with gene repression[18,19]. In *Saccharomyces cerevisiae*, the yeast orthologue of H2A.Z, Htz1, is acetylated by NuA4 lysine acetyltransferase (KAT)[20,21]. The mammalian orthologue of NuA4, Tip60/Kat5, is a member of MYST family of KATs and is primarily recognized

for targeting core histones H4 and H2A, including in the neuronal tissues[22-27]. Increasing evidence suggests a link between Tip60 and acetylation of H2A variants, including H2A.Z[28-31]. However, the direct role of acetylation and its contribution to H2A.Z function during gene regulation and cell fate specification has not been addressed.

Here, we set out to identify the key chromatin remodeling complexes that are recruited by proneural TFs to activate chromatin and enable neuronal cell fate specification. We found Tip60 acetyltransferase as critically required for neuronal induction during direct lineage conversion and neuronal differentiation. The mechanism by which Tip60 mediates neuronal specification involves acetylation of histone variant H2A.Z. Remarkably, H2A.Zac is dispensable for overall function of H2A.Z in regulating active transcription and chromatin structure. Instead, it is selectively required for the activation of a subset of silent, lineage-restricted genes marked by bivalent chromatin signature.

Results

Identification of a neuronal lineage-determining transcription factor interactome

To identify the key chromatin factors that establish neuronal identity we determined the protein-protein interaction (PPI) network of the three proneuronal TFs, Ascl1, Brn2, and Myt1l, using three experimental approaches (Figure S1A-B). First, we used the well characterized G-LAP-Flp targeting system to purify LAP-tagged (EGFP-TEV-S-peptide-tagged) versions of the three TFs from T-Rex™ HEK293 cells[32]. Second, we identified proteins that associate with the three factors directly in MEFs, since their combined expression induces neuronal identity in this cell type[15]. Here, we employed in parallel BioID proximity labeling and tandem affinity purification using BirA- or FLAG/His[7]-tagged TFs, respectively (Figure 1A, S1A-B)[33]. Mass spectrometry analysis of isolated protein complexes revealed that each factor co-purified with several hundred proteins (Figure S1A, Table S1). All three factors shared a pool of interacting partners representing a candidate set of common co-regulators of neuronal specification (Figure S1C). Among the proteins identified in the screens were proteins previously reported to interact with Ascl1 (e.g. Tcf3-12 or Huwe1)[34,35], Myt1l (e.g. Sin3b)[36] and Brn2 (e.g. Yap1)[37]. Majority of the hits, however, are new candidate binding proteins.

The neuronal specification protein network contains multiple acetyltransferases

To explore our datasets and interrogate functional connections among the candidates we supplemented the mass spectrometry results with known interactions from the BioGRID database[38]. We assembled the resulting dataset into an interactome map using Cytoscape[39], thereby obtaining a high-confidence neuronal fate specification network composed of ~800+ proteins (see also Methods). Gene ontology (GO) enrichment analysis revealed that the network proteins could be grouped into multiple functional modules (Figure 1B, Table S2). One of the larger modules (294 proteins) was enriched in GO terms associated with histone acetylation. Given the link between acetylation and gene activation we decided to explore the potential role of this group of candidates in neuronal induction. Notably, thirty of the proteins in this cluster were either acetyltransferases or subunits of specialized multiprotein acetyltransferase complexes (Figure 1C). Among these, three of the MYST

lysine acetyltransferases, Tip60/Kat5, Hbo1/Kat7 and Mof/Kat8, drew our attention in particular (Figure 1D). The MYST proteins have been critically implicated in regulating multiple aspects of mammalian development[25,26,40-46], and several of them, including Tip60 and Mof, were linked to neurodevelopmental disorders, including cerebral malformations and intellectual disability[23,47]. As little is known about the role of these proteins in cell fate transition, we decided to explore their function in neuronal induction.

Tip60 is a general gate keeper of neuronal cell identity

To investigate the functional involvement of MYST acetyltransferases in neuronal specification we analyzed how RNAi-mediated depletion of Tip60, Mof and Hbo1 impacts Ascl1's ability to induce neuronal identity in TauGFP reporter MEFs (Figure 1E-F). Five days following Ascl1 expression the TauGFP induction in cells co-transduced with Hbo1 and Mof shRNAs was comparable to TauGFP induction in the control cells (Figure 1E). In contrast, knockdown of Tip60 resulted in a striking, ~80% reduction in TauGFP$^+$ cells on day 5, and absence of MAP2$^+$ neurons on day 14 of neuronal induction (Figure 1E, Figure 2A-C). RNAi-mediated knockdown of several other subunits of the NuA4/Tip60 complex detected in affinity purification and BioID experiments impaired the induction of TauGFP to a similar degree (Figure 1G and S1D), suggesting a requirement for NuA4/Tip60 complex for neuronal fate specification. Introduction of *TIP60* cDNA that is resistant to Tip60 RNAi restored Ascl1-mediated neuronal induction in the knockdown cells (Figure S2A-D). To further validate the RNAi effects, we generated a Tip60 conditional knockout (cKO) mouse (Figure S2E-H). Indeed, Cre-mediated deletion of Tip60 in cKO fibroblasts impaired the generation of neurons in response to Ascl1 (Figure S2I). Tip60 knockdown did not inhibit lentiviral expression of Ascl1, which instead remained increased throughout the reprogramming (Figure 2B)[48]. Higher efficiency reprogramming systems, such as those that include Brn2 and/or Myt1l in addition to Ascl1, or those that comprise factor combinations without Ascl1[14,16,17], all failed to override the reprogramming block imposed by Tip60 depletion (Figure 2D-H). Additionally, knockdown of Tip60 in Ascl1-inducible mouse embryonic stem (mES) cells prevented the formation of neurons also in this system, even though TF-mediated differentiation is extremely efficient and robust in pluripotent stem cells (Figure S2J-M)[49]. Notably, knockdown of Tip60 also impaired the conversion of fibroblasts into muscle-like cells by MyoD1 TF, suggesting that Tip60 function in fate specification is not restricted to neuronal lineage (Figure S2N-P). Finally, we found that Tip60 is needed for physiologic neuronal differentiation from embryonic neural precursor cells (NPCs) (Figure 2I-N). Thus, Tip60 function constitutes a requirement for neuronal fate specification and perhaps for cell fate transition in general.

Tip60 depletion affects early steps of neuronal induction

To distinguish at which stage the Tip60 knockdown perturbs neuron formation, we took advantage of an inducible CRISPR/Cas9 system, which relies on the reversible regulation of destabilizing domain (DD)-Cas9 fusion protein by the Shield-1 ligand, to deplete Tip60 at different times during neuronal induction (Figure S3A-C)[50]. We tested the effects of various three day-long periods of Shield-1 treatment (Figure S3D). Tip60 depletion during the first three days blocked TauGFP induction and generation of TUJ1$^+$ neurons (Figure S3E-G). However, as the Shield-1 treatment was progressively delayed, the impact of Tip60

inactivation on neuron formation became less severe, with day 10 treatment having no apparent effects (Figure S3E-F). Late and continuous inactivation of Tip60 did not affect neuronal stability when analyzed at day 21 post-induction, i.e., 11 days after Tip60 depletion (Figure S3E-F). This suggests that the major role of Tip60 is at the initial steps of the cell identity transition, as opposed to maturation and maintenance of already formed neurons.

Given the reported involvement of Tip60 in regulating cell viability and proliferation[26,51-54], we investigated whether Tip60 effects on these parameters could explain the lack of neuron formation. The block in TauGFP was observed as soon as 48h post-induction (Figure S3H-J). Up to that point, however, we did not observe Tip60-dependent changes in apoptosis, with increased Annexin V staining detected only at day 5 (Figure S3H-J). Loss of Tip60 was reported to lead to a complete cell cycle arrest in actively dividing cells[55]. Tip60 depletion in our system also caused a decrease in the fraction of $Ki67^+$ cells, suggesting an accelerated cell cycle exit (Figure S3H). However, BrdU incorporation and DNA content analysis at different times of neuronal induction revealed no significant differences in cell cycle phase distribution between the control and Tip60-deficient cells up to day 5 of neuronal induction (Figure S3K). Importantly, under the culture and viral transduction conditions used during reprogramming, both the control and Ascl1-transduced MEFs ceased to cycle nearly completely. This suggests that any possible cell cycle-related effects of Tip60 are largely concealed in our system. Furthermore, pan-cyclin inhibitor SU9516 treatment, which mimics the increased cell cycle exit rate[51,56,57], resulted in an increase in $TauGFP^+$ cells in control, but had no effect on neural induction in Tip60 depleted cells (Figure S3L). We therefore concluded that the effects of Tip60 on cell survival or proliferation could not fully explain the neuronal induction failure.

Tip60 relies on its acetyltransferase activity and chromodomain to promote neurogenesis

Next, we sought to understand the mechanism of Tip60 function. To this end we introduced a series of point or deletion mutations disrupting specific Tip60 domains to test whether the mutant proteins could rescue Tip60 knockdown effects (Figure 3A, see also Methods). After confirming that the mutant proteins were stable and localized to the nucleus (Figure S4A-B), we co-expressed them with the control or Tip60 shRNAs in Ascl1- or Brn2/Ascl1/Myt1l-expressing cells. Only mutations disrupting acetyltransferase- or chromo- domains abrogated Tip60 function and conferred dominant-negative effects on Tip60 in the absence of RNAi (Figure 3A-B and S4D-F). Notably, Tip60's chromodomain has been postulated to mediate binding to methylated histone tails[24,58], suggesting that Tip60 exerts its primary function during neuronal specification by recruitment via its chromodomain and acetylation of target proteins on chromatin.

H2A.Z acetylation is critical for neuronal specification and is mediated primarily by Tip60

We next sought to identify Tip60 targets relevant for neuronal induction. To date, many non-histone and histone proteins have been shown to be substrates of Tip60. Among histones, H4 and H2A were suggested as primary Tip60 targets in yeast and mammals[53,59,60]. Accordingly, we observed a subtle, but reproducible decrease in acetylation of histone H4 and H2A upon Tip60 RNAi, while H3 acetylation remained largely unaffected (Figure S5A-B). However, while exploring additional candidate substrates, we found that Tip60 depletion

resulted in a nearly complete, global loss of H2A.Zac (Figure 3C-E and S5C). These striking results were confirmed in Tip60 cKO cells (Figure S5D-E). H2A.Zac was dependent on Tip60 also in other cellular contexts, including primary NPCs and mES cells (Figure 3F and S5F). Notably, NuA4/Tip60 complex has another biochemical activity involved in the regulation of H2A.Z that is encoded by Ep400 ATPase, an enzyme responsible for H2A.Z deposition through histone exchange[61]. Knockdown of Ep400 resulted in a strong H2A.Zac decrease (Figure S5G-H), consistent with the notion that intact NuA4/Tip60 is required for proper H2A.Z regulation and neuronal induction. Recombinant Tip60 directly acetylated H2A.Z in a dose- and acetyl-CoA-dependent manner *in vitro* (Figure 3G). In contrast to wild type (WT) Tip60, loss of H2A.Zac could not be restored by acetyltransferase-deficient mutant of Tip60 (Figure 3D-E). The chromodomain mutant was only partially effective in restoring H2A.Zac, suggesting that the chromodomain-mediated recruitment of Tip60 to chromatin may facilitate histone acetylation (Figure 3D-E)[24,58]. Given that the expression of other key KATs was unaffected (Figure S5I), we concluded that Tip60 is the acetyltransferase responsible for the bulk of the H2A.Zac.

Next, we explored the function of H2A.Zac in neurogenesis. The induction of neuronal fate is accompanied by an increase in H2A.Zac that persists throughout the neuronal induction (Figure 4A-B). Accordingly, the level of H2A.Zac in TauGFP^{+} cells was significantly higher than that found in TauGFP^{-} cells, demonstrating dynamic regulation of H2A.Zac during the establishment of neuronal identity (Figure 4C-D). H2A.Z RNAi exerted a dose dependent inhibitory effect on neuron formation (Figure 4E-F and S5J). To assess the role of H2A.Zac, we generated an acetylation-resistant H2A.Z (H2A.Z^{KR}) by mutating all five of H2A.Z' N-terminal lysines to arginines (Figure 4G)[62]. Both H2A.Z^{WT} and H2A.Z^{KR} expressed at similar levels and were efficiently incorporated into chromatin (Figure 4H and S5K). Ectopic expression of H2A.Z^{WT} and H2A.Z^{KR} resulted in a decrease in the amount of endogenous H2A.Z, suggesting that overexpressed H2A.Z effectively competed with endogenous protein on chromatin (Figure 4I). Importantly, this genomic incorporation of H2A.Z^{KR} significantly impaired the formation of neurons (Figure 4J-K). Thus, H2A.Z acetylation mediated by Tip60 is essential for proper neuronal cell fate specification.

Tip60 and H2A.Zac primarily mark promoters and are dynamically regulated during neuronal differentiation

To begin exploring how Tip60-mediated H2A.Zac induces lineage specification, we used Cut&Tag to obtain genome-wide occupancy profiles of Tip60, H2A.Z and H2A.Zac (Figure S6). In fibroblasts, Tip60 and H2A.Zac showed highest enrichment at active promoters, in contrast to H2A.Z sites with no overlapping H2A.Zac (Figure S6A-C). Consistent with our functional results, most of the Tip60 peaks overlapped with H2A.Zac (10,652 out of 11,865 peaks) (Figure S6D). Genomic sites with both Tip60 and H2A.Zac enrichment (the Tip60^{+}/H2A.Zac^{+} sites) were highly enriched at transcription start sites (TSSs), in contrast to Tip60^{+}/H2A.Zac^{-} and Tip60^{-}/H2A.Zac^{+} peaks (Figure S6A-B). The ~2/3 of H2A.Zac peaks that showed no significant Tip60 co-enrichment displayed significantly lower acetylation levels and marked predominantly non-TSS regions (Figure S6A and S6E-left). Their enrichment also decreased upon Tip60 knockdown (Figure S6E-right),

suggesting that Tip60 may be below the detection level at these sites, or another KAT contributes to weaker H2A.Z acetylation[28,63].

Neuronal induction led to substantial rearrangements of Tip60, H2A.Z and H2A.Zac occupancy. In line with our immunoblotting results, the number of H2A.Zac peaks increased with neuronal differentiation (Figure S6F-G). Over 85k genomic loci changed enrichment of H2A.Z and/or H2A.Zac by day 5 post-Ascl1 induction (Figure S6G-H). 7% (6093) of all changes occurred at TSS's, with a change in H2A.Zac/H2A.Z ratio marking changes in expression of 1038 genes (Figure S6I).

Tip60 RNAi did not have a substantial effect on global H2A.Z distribution: we failed to identify genomic sites that have significantly changed H2A.Z enrichment upon Tip60 RNAi in day 2 Ascl1-iN cells (fc≥2, padj<0.05). Accordingly, the average enrichment of H2A.Z at Tip60 binding sites remained unaffected by Tip60 RNAi (Figure S6J). This further suggests that under our experimental conditions Tip60 inactivation did not appreciably disrupt the H2A.Z incorporation activity assigned to other subunits of the NuA4 complex[61,64].

Across all conditions, enrichment of H2A.Zac and Tip60 strongly correlated with transcriptional activity and enrichment of other active histone marks (Figure S6K-N).

H2A.Z acetylation is dispensable for the overall gene activity

Having identified the main acetyltransferase responsible for H2A.Zac we were now able to test whether the correlation between H2A.Zac and active gene transcription is of functional relevance. To that end, we performed RNA sequencing (RNA-seq) at days 2 and 5 of Ascl1 induction in fibroblasts, with and without Tip60 (Figure S7A). Strikingly, despite a nearly complete loss of H2A.Zac, the gene expression in day 2 cells remained largely unaffected by Tip60 RNAi (Figure 5A): although Ascl1 induction altered the expression of 937 genes, only 110 genes were deregulated in Tip60-depleted Ascl1 cells (Figure 5B-left). Of those, many were associated with cell adhesion or proliferation-related GO terms (Figure 5C). To exclude the possibility that the knockdown effects are 'overridden' by the ectopic expression of the strong transcriptional activator Ascl1, we analyzed gene expression profiles of normal fibroblasts with and without Tip60 depletion. To mimic the lack of active cycling observed during neuronal induction, MEFs were plated at the same density and not passaged after reaching confluency, thereby preventing the reactivation of proliferation. However, we found again only modest transcriptional changes even after extending the duration of Tip60 knockdown to 7 days (Figure S7B-D).

Tip60 is required for the suppression of fibroblast identity

The modest effects on transcription after near complete loss of H2A.Zac at day 2 were in stark contrast to the strong inhibition of neuronal induction. Accordingly, Tip60-dependent transcriptional changes became more prominent at later times of reprogramming, with Tip60 RNAi disrupting the expression of over 1100 genes by day 5 (Figure 5A, 5B-right, 5D). We therefore sought to explore whether Tip60 regulates cell identity transitions rather than steady-state transcription. More specifically, we asked whether Tip60-deficient cells retain their fibroblast identity even after exposure to strong neuronal lineage inducers. Indeed, GO term analysis of significantly deregulated genes on day 5 indicated lack of

neuronal gene induction and retention of fibroblast gene expression (Figure 5C). TF analysis by ISMARA[65] revealed that Tip60 depletion disrupts activity of several transcriptional regulators (Figure 5E), including the overactivation of the neuronal lineage repressor Rest[66]. Accordingly, 23 out of 78 high confidence Rest targets failed to be de-repressed in Tip60-deficient cells (Figure 5F-G). GSEA revealed that the fibroblast-specific gene expression signature was strongly enriched in day 5 Tip60-deficient cells (Figure 5H and S7E, Table S4), and fibroblast-specific genes that are normally silenced during neuronal specification were upregulated upon Tip60 RNAi (Figure 5I). At the same time, we did not find evidence of induction of other, alternate cell fates, or enhanced induction of muscle program, despite higher Ascl1 levels detected in Tip60-deficient cells (Figure 2B) and the reported ability of this TF to induce myogenic gene expression in MEFs[48] (Figure S7F-G).

We previously established that the fibroblast to neuron cell identity change is associated with a coordinated chromatin ‘switch’ that occurs between days 2 and 5 of neuronal specification by Ascl1[16]. Remarkably, despite the close correlation between H2A.Zac and chromatin accessibility, most of the ATAC-seq changes induced by Ascl1 on day 2 were not affected by Tip60 knockdown and loss of H2A.Zac (1,277 out of 68,693 of day 2 sites were affected) (Figure 5J and S7H), and the perturbed accessibility became evident only at later times (14,512 affected sites at day 5). Notably, knockdown of H2A.Z had more prominent effect on chromatin structure affecting over 5k sites in day 2 shH2A.Z-transduced cells, suggesting that likely H2A.Z deposition, and not its acetylation, is the primary determinant of chromatin accessibility (Figure S7I). It is noteworthy, however, that just like in case of Tip60, many of the H2A.Z effects are linked to its role in cell cycle, and thus are less evident at early stages of neuronal induction in MEFs[67]. We next examined ATAC-seq dynamics at fibroblast- vs neuron-specific chromatin sites in shTip60 cells. We discovered that Tip60 depletion effectively blocked the chromatin ‘switch’ at 15% of these sites (6,113 sites), with day 5 knockdown cells failing to gain accessibility at neuron-specific sites and retaining elevated accessibility at fibroblast-specific sites (Figure 5J-K, Table S3). Thus, without Tip60 and H2A.Zac fibroblasts fail to change their transcriptional and epigenetic identity.

Ascl1 recruits Tip60 to chromatin to induce silent Ascl1 targets

Next, we sought to define the direct molecular actions of Tip60 at its target sites during neuronal induction. Given our finding of the interaction between Tip60 and Ascl1, we investigated if Tip60 loss affects function of Ascl1. Although Tip60 predominantly occupies promoter regions in fibroblasts, neuronal induction drove its enrichment primarily at distal regulatory elements (Figure 6A). Sites gaining Tip60 were enriched for the E-box motif, a motif that is also recognized by Ascl1 (Figure 6B). Notably, Ascl1 binds predominantly distal enhancers[17] suggesting that Ascl1 recruits Tip60 to chromatin. Indeed, 62% (369 out of 594) of Tip60 peaks induced at day 2 overlapped with Ascl1 binding sites, and 32% (1733 out of 5371) of the Ascl1-occupied sites were co-bound by Tip60 during at least one of the neuronal induction time points (Figure 6C). Thus, Ascl1 is largely responsible for the increased Tip60 binding at distal enhancers.

Next, we examined if Tip60 RNAi affects Ascl1 activity during neuronal specification. As expected, Ascl1/Tip60 co-bound sites failed to gain H2A.Zac, but not total H2A.Z (Figure

6D). We then examined the expression of a set of core Ascl1 target genes. Only a subset of these failed to be properly induced upon Tip60 depletion, while the others remained unaffected or even induced more strongly (Figure 6E). While examining the genes with impaired induction, we found that most of them were silent in fibroblasts and thus not expressed at the start of reprogramming (‘off’ genes, average FPKM<1, see also Methods). The ‘on’ genes, which are active and expressed in fibroblasts (FPKM≥1), were largely unaffected by Tip60 RNAi (Figure 6E-G, Table S5).

Tip60 is required for the induction of late & silent neuronal program

We next asked whether the association between gene activity and Tip60 dependence is restricted to Ascl1 targets or is a more general phenomenon affecting all genes induced during neuronal specification, regardless of Ascl1 binding. To this end, we categorized all induced genes into ‘on’ and ‘off’ groups based on their expression in the starting fibroblast population, and further subdivided the latter into genes that are induced ‘early’ or ‘late’ (Figure 6H, top). Similarly, repressed genes were classified into ‘transient’, ‘early’ and ‘late’ (Figure 6H, bottom). None of these groups were significantly affected by Tip60 knockdown, except for the ‘off’/‘late’ group, which failed to properly induce upon Tip60 depletion (Figure 6H). Thus, Tip60 is specifically required for the proper activation of neuronal genes that are well silenced and activated slowly, but not for general up- or downregulation.

Tip60 and H2A.Zac promote H3K4me3 deposition and promoter activation

To understand how Tip60 regulates induction of the ‘off’ genes, we compared Tip60 and H2A.Zac occupancy with other chromatin features at enhancers and promoters of the ‘on’/‘off’ Ascl1 target genes (Figure 6I). Enhancers of both gene groups displayed similar patterns of Tip60 and H2A.Zac enrichment and showed reduced H2A.Zac upon Tip60 knockdown (Figure 6I). Loss of H2A.Zac did not perturb chromatin accessibility at any of these loci (Figure S6O), further indicating that H2A.Zac does not directly regulate chromatin accessibility. As expected, the ‘on’ promoters displayed higher Tip60, H2A.Zac enrichment and chromatin accessibility at the start of neuronal induction, while the ‘off’ genes began to acquire them only after the onset of induction. These observations further support the notion that Tip60/H2A.Zac, although not required to maintain active transcription, could be necessary for establishing transcriptional competence for silent gene activation.

To explore this further, we compared the dynamics of H3K4me3, an active promoter mark, at the ‘on’ and ‘off’ promoters of Ascl1 targets (Figure 6I) and among all Tip60-regulated genes induced during neuronal specification (Figure 6J). Reflecting their transcriptional states, the promoters of the ‘off’ genes showed a ~10-fold lower H3K4me3 enrichment in control fibroblasts (Figure 6I). Somewhat surprisingly, the ‘on’ promoters showed no H3K4me3 increase as the genes became induced over time. In contrast, the ‘off’ promoters gradually gained H3K4me3 throughout the neuronal induction (Figure 6I-J). This suggests that distinct mechanisms drive the transcriptional upregulation between the two groups of genes. Inactivation of Tip60 interfered with the gain of H3K4me3 at the ‘off’ gene promoters, while it had no effect on H3K4me3 on the ‘on’ gene promoters (Figure 6I-J). Thus, Tip60-mediated H2A.Zac is necessary for the increase in promoter H3K4me3 and transcriptional activation of the significant subset of the ‘off’ class of genes.

Tip60 and H2A.Zac are required for the activation of bivalent domains

We next sought to explore whether a specific chromatin signature is associated with Tip60/H2A.Zac-dependent gene regulation. ChromHMM analysis of Tip60-dependent 'off' promoters revealed enrichment of two unique chromatin states (states 7 and 9) (Figure 7A). Both states were co-enriched in H3K4me3 and H3K27me3, which is a characteristic of the bivalent promoters[68-70] (Figure 7A, S7J-K). State 7 had essentially no H2A.Zac enrichment and less H3K4me3 leading to a higher H3K27me3:H3K4me3 ratio, and therefore being characteristic of a more repressed state (Figure 7A-B)[71]. Thus, the subset of silent genes that are induced late during neurogenesis and specifically depend on Tip60 for activation are characterized by a bivalent promoter configuration.

Tip60/H2A.Zac-dependent activation of the bivalent gene *Miat* is critical for proper neuronal induction

We next wondered whether the failed activation of a subset of bivalent genes could explain the strong inhibition of neuronal specification. Out of the bivalent Ascl1 targets, 26% of state 7 and 18% of state 9 genes failed to properly induce in the absence of Tip60, with most strongly affected genes displaying the highest H3K27me3:H3K4me3 ratios at their TSS (Figure S7L). One of these 'off' genes is the neuronal specification-induced lncRNA, Myocardial Infarction-Associated Transcript (*Miat*). Its promoter region is marked by a bivalent chromatin signature that is enriched in H2A.Zac, resembling state 9 (Figure 7E). Remarkably, Tip60 depletion essentially eliminated transcriptional activation and H3K4me3 deposition at the *Miat* promoter (Figure 7C and 7E). Expression of acetylation-resistant H2A.Z^{KR} also interfered with induction of *Miat* (Figure 7D), indicating that Tip60-dependent H2A.Zac is necessary for proper *Miat* activation. Importantly, RNAi-mediated knockdown of *Miat* triggered a dose-dependent inhibition of TauGFP induction and TUJ1^{+} neuron formation demonstrating that *Miat* is important for neuronal induction (Figure 7F-G). Thus, Tip60-dependent activation of a subset of bivalent genes is critical for neuronal specification.

Discussion

Establishment of a chromatin environment that is permissive for cell fate transition is governed by a complex interaction between sequence-specific TFs and chromatin modifying complexes[4,5,72]. Here we demonstrate that the Tip60 acetyltransferase is recruited to chromatin by neuronal lineage-determining TFs, and its recruitment is critically required for neuronal fate induction via acetylation of the histone variant H2A.Z.

Tip60 participates in a variety of cellular processes, including stress response, cell cycle, apoptosis, or DNA repair[53,73]. Accordingly, we found that Tip60 depletion has pleiotropic biological effects, and thus Tip60 likely regulates neuronal induction by multiple mechanisms. For instance, Tip60 was shown to be required for neuronal viability in the mouse cortex where its inactivation caused apoptosis and neuronal loss 3 weeks after Tip60 deletion[26]. In our hands, Tip60 loss-of-function also triggered apoptosis in fibroblasts induced to become neurons, though decrease in acetylation, gene expression changes and reprogramming failure were detected before the onset of apoptosis. Similarly, much of

the Tip60 effects on cell cycle seem to be concealed in our reprogramming system, but we are not able to fully exclude a potential mis-regulation of cell cycle signaling and its contribution to Tip60 function in neuronal specification.

Tip60-dependent gene regulation has been mainly attributed to Tip60-mediated acetylation of core histones H2A and H4. We found that Tip60 depletion had only subtle effects on these histones during neuronal induction, whereas the impact on H2A.Zac was much more pronounced. Intriguingly, our data suggest that additional mechanisms could contribute to H2A.Zac. We observed that loss of H2A.Zac is not restricted to Tip60 occupied loci, and Cre-mediated knockout of Tip60 does not completely abolish H2A.Zac. Among histone acetyltransferases (HATs), CBP/Ep300 and GCN5/Kat2a were reported to target H2A.Z in other contexts[28,63], and cooperative interaction between Tip60 and Ep300 has been noted in regulating acetylation during immune responses[74]. Nevertheless, in the context of our study Tip60 is responsible for inducing and/or maintaining a bulk of H2A.Zac, as its depletion caused ~80% reduction in global H2A.Zac.

Our data indicate that Tip60/H2A.Zac are dispensable for maintaining or regulating active transcription. This is particularly striking given the steady-state occupancy of Tip60 at virtually all active promoters and high correlation between Tip60 enrichment, H2A.Zac and gene expression. Notably, this pattern of binding is common for many HATs, suggesting a high level of redundancy in maintaining acetylation at active TSS[75]. Furthermore, it is becoming apparent that there is a great degree of functional redundancy among acetylation sites on histones as well, and a debate regarding a degree to which a specific acetylation site matters, as opposed to maintaining a certain level of acetylation on the nucleosome, in general[76]. Despite of the above, we uncovered a small subset of silent neuronal genes that are highly sensitive to Tip60/H2A.Zac loss. Notably, these bivalent genes are enriched for critical regulators of neurogenesis (e.g., *Miat*), suggesting that their activation is key for the pioneering function of Ascl1 in inducing neuronal identity.

Bivalent chromatin domains are best recognized for their involvement in developmental regulation in pluripotent stem cells, where they mark key developmental gene promoters and enhancers that are poised for activation[77,78]. However, increasing evidence suggests that they may represent a universal mechanism for lineage-specific gene regulation, as bivalent domains have been now also described in fibroblasts, neural progenitors, hematopoietic progenitors and other cell types[69,79-83]. How bivalency is resolved into monovalent domains during differentiation remains unclear. Tip60-mediated H2A.Zac, as shown here, may play an important part in this process. We found that the bivalent gene activation and the associated H3K4me3 gain critically depend on a functional Tip60. Whether the increase in H3K4me3 is in fact instructive for more transcription remains a matter of debate, since increasing evidence suggests that the primary function of H3K4me3 is to repel active repression, as opposed to a causative role in gene activation[84-86]. This is in line with observations that H3K4me3 enrichment itself does not always correlate well with transcriptional activity, but rather erasure of this mark leads to elevated H3K27me3 and DNA methylation[84,86,87].

Notably, de-regulation of H3K4me3 is thought to lie at the core of many disorders of the developing brain[88,89]. Strikingly, *de novo* missense mutations in *KAT5* have been recently linked to neurodevelopmental syndrome that is characterized by progressive cerebellar atrophy and CNS malformations, resulting in severe developmental delay and intellectual disability[23]. It will be interesting to explore how the perturbations in H3K4me3 deposition and bivalent chromatin caused by Tip60 loss-of-function contribute to the overall phenotype in the affected individuals.

In summary we identified previously unknown function of Tip60-mediated H2A.Zac in bivalent gene activation during neuronal cell fate induction. Tip60 has been shown to regulate cell identities in multiple cell types[22,90-92]. Thus, our results raise the possibility that the Tip60/H2A.Zac-dependent mechanism of bivalent chromatin regulation is critical not only during neuronal specification, but for cell fate transitions in general.

Limitations of the study

Given the pleiotropic biological effects of Tip60 we were not able to assess the extent to which other molecular functions of Tip60 contribute to its effects on reprogramming. In addition, Tip60-dependent gene promoters are enriched for bivalent chromatin signature. The bivalent signal, however, may also arise from the heterogeneity of chromatin landscape within the cell population, as we have not established bivalency using individual nucleosome assays or sequential ChIP.

STAR Methods

RESOURCE AVAILABILITY

Lead contact—Further information and requests for resources and reagents should be directed to and will be fulfilled by the lead contact, Marius Wernig (wernig@stanford.edu).

Materials availability—Reagents generated in this study are listed in key resources table and are available upon request.

Data and code availability

- RNA-seq, ATAC-seq and Cut&Tag data generated in this study have been deposited at the Gene Expression Omnibus (GEO) database under super series accession number GSE181965. The accession numbers for existing, publicly available datasets used for the analyses are listed in the key resources table.
- This study does not report original code.
- Any additional information required to reanalyze the data reported in this paper is available from the lead contact upon request.

EXPERIMENTAL MODEL AND SUBJECT DETAILS

Animal model—All mouse studies were performed according to protocols approved by the Stanford University Administrative Panel on Laboratory Animal Care and conformed to NIH Guidelines for the Care and Use of Laboratory Animals. All mice were housed in the

Stanford animal facility under the supervision of Stanford animal care unit; all mice were healthy and not kept in a sterile facility. Mouse strains used and generated in this study are listed in the key resources table.

Primary cell cultures—Primary cells were derived from embryonic day (E)13.5 old mouse embryos obtained from 8–24-week-old pregnant females. Mouse embryonic fibroblasts (MEFs) were isolated from heterozygous TauGFP knock-in mouse embryos[94] (Jackson Laboratory, RRID:IMSR_JAX:004779) or from homozygous Tip60/Kat5 conditional knockout (cKO) embryos (generated in this study). Neural precursor cells (NPCs) were isolated from the cortices of the homozygous Rosa26::CAG::SpCas9-P2A-EGFP mouse embryos (Jackson Laboratory, RRID:IMSR_JAX:024858). Feeder cells were derived from CD1(ICR) (Charles River, RRID:IMSR_CRL:022) or DR4 mice (Jackson Laboratories, RRID:IMSR_JAX:003208). Embryos of both sexes were used.

Cell lines—Male mouse embryonic stem cells (v6.5[95]) were maintained in a 5% CO_2 environment at 37°C as described in the Method section below.

METHOD DETAILS

Cell derivation and Maintenance—Homozygous TauGFP knock-in mice[94] (Jackson Laboratory, RRID:IMSR_JAX:004779) were bred with C57BL/6J mice (Jackson Laboratory, RRID:IMSR_JAX:000664). Mouse embryonic fibroblasts (MEFs) were isolated from heterozygous E13.5 TauGFP knock-in embryos as previously described[15] and maintained in DMEM (Gibco) supplemented with 10% cosmic calf serum (CCS, Thermo Fisher Scientific). Neural precursor cells (NPCs) were isolated from cortices of Rosa26::CAG::SpCas9-P2A-EGFP mouse embryos (Jackson Laboratory, RRID:IMSR_JAX:024858) at E13.5 and maintained as a monolayer on polyornithine/laminin coated plates in DMEM/F12 (Gibco) containing N2 and B27 supplements (Gibco), 20 ng/ml EGF (R&D Systems) and 10 ng/ml FGF (Peprotech).

v6.5 mouse embryonic stem cells (mESCs)[95] were maintained on mitomycin C-treated feeder cells obtained from CD1(ICR) mice (Charles River, RRID:IMSR_CRL:022) in DMEM supplemented with 12 % knockout replacement serum (Invitrogen), 3% cosmic calf serum (Thermo Fisher Scientific) and LIF.

Cell line generation—To generate Ascl1-inducible murine ES line, v6.5 mESCs were dissociated using 0.05% trypsin/EDTA and resuspended in HBSS (Sigma). 20 μg of Piggybac-Ascl1[96] and 10 μg of transposase vector (System Biosciences, CA) were mixed with the cell suspension in a 0.4-cm cuvette (Bio-Rad) and electroporated using a Bio-Rad Gene Pulser. Cells were re-plated onto mitomycin C-treated feeder cells obtained from DR4 mice (Jackson Laboratories, RRID:IMSR_JAX:003208) and maintained in selection media until stably growing colonies were observed. Individual colonies were picked and tested for expression of Ascl1.

Flp-In T-Rex™ HEK293 cell line was obtained from Invitrogen. Stable cell lines expressing LAP-tagged transcription factors (TFs) were created as previously described[97]. Briefly,

pG-LAP constructs encoding TFs (see below) were co-transfected with pOG44 (Invitrogen) using Fugene6 (Roche) and selected for stable integrants with puromycin.

Generation of Tip60 conditional knockout mice—Heterozygous Tip60/Kat5 conditional knockout (cKO) v6.5 mESCs were generated by flanking first two exons of the *Kat5* gene by locus of X-over P1 (loxP) sites (Figure S2E-G) using CRISPR-Cas9/RNP and double stranded donor-mediated homologous recombination. The targeting vector was designed to contain two homology arms separated by a selection cassette containing a splice acceptor (SA) followed by an internal ribosomal entry site (IRES) and the Neomycin resistance gene (NeoR) with a polyadenylation signal (pA). v6.5 cells, which for this purpose were maintained on feeder cells in DMEM containing 15% fetal bovine serum (HyClone) and LIF, were harvested with trypsin/EDTA. 30 μg of SpCas9 protein (Integrated DNA Technologies) and 16 μg of synthetic single guide RNA (sgRNA, Synthego) were mixed in 30 μl of OptiMEM (Thermo Fisher Scientific) and incubated 15 min at RT. The mixture was subsequently diluted with 70 μl OptiMEM containing $2.5x10^6$ cells and 2 μg of targeting vector, which was linearized by cutting with BsaI (NEB), and nucleofection was performed using Nucleofector™2b (Lonza). The cells were selected for 5 days in medium containing G418 Sulfate (Gibco), drug-resistant clones were picked, and correct homologous recombination was identified by PCR followed by Sanger sequencing. All positive integrations were heterozygous, consistent with the previous reports that loss or strong depletion of Tip60 disrupts mES cell self-renewal[41,90]. Selection cassette was removed from three positive clones by transient expression of FlpE recombinase.

To produce chimeric mice, Kat5 cKO mESCs were microinjected into the blastocyst-stage embryos isolated from C57BL/6J females (Jackson Laboratory, RRID:IMSR_JAX:000664) using piezo-actuated microinjection pipette, and the injected blastocysts were transplanted into the uterus of day 2.5 pseudo-pregnant recipient CD1(ICR) female mouse (Charles River, RRID:IMSR_CRL:022). Caesarean section was carried out at day 19.5 and pups were fostered by lactating ICR mothers. Resulting chimeras were bred with C57BL/6J mice, offspring genotyped by PCR of tail tip DNA and F1 mice carrying the mutant allele were intercrossed to obtain homozygous Kat5 cKO mice. Cre-dependent inactivation of Tip60 was further confirmed by immunoblotting following transduction with Cre or ΔCre (truncated and non-functional version of Cre used as a control) expressing lentivirus (Figure S2H).

Tip60 cKO MEFs were derived from homozygous mutant E13.5 embryos and maintained as described above.

DNA constructs—FUW-TetO lentiviral vectors encoding doxycycline-inducible Ascl1, Brn2, Myt1l, Ngn2, Zfp238 and MyoD1 were described previously[15,17,49,98]. Sequences encoding Brn2, Ascl1, full length Myt1l ($Myt1l^{FL}$) and minimal active Myt1l truncation ($Myt1l^{200–623}$)[36] tagged at their N-termini with $FLAG/His^7$ tandem epitope or BirA* tags, full length human Tip60 cDNA tagged at its N-terminus with HA-tag, as well as Tip60 point and deletion mutants (see below) were generated by PCR and subcloned into FUW-TetO. Lentiviral vector expressing DD-Cas9-P2A-Puro (pEDCPP) was derived from pEDCPV (gift from R. Sordella[50]) by replacing Venus sequence with a PuroR coding sequence.

shRNA oligonucleotides were cloned into pSico-Puro (gift from T. Jacks), and sgRNAs targeting *Kat5* gene locus (sgRNA#3-#5) were cloned into pLentiGuide[99] (Addgene plasmid # 117986) or pEDCPP. Sequences of shRNA and sgRNA used are listed in Table S6. Wild type H2A.Z.1 cDNA (H2A.Z^{WT}) and acetylation-resistant mutant of H2A.Z.1 (H2A.Z^{KR}, carrying five lysine to arginine substitutions: K4R, K7R, K11R, K13R, K15R), tagged at their C-termini with HA-tag were synthesized as geneBlocks by IDT and cloned into FUW-TetO. For experiments involving Tip60 cKO cells, lentiviral vectors encoding NLS-EGFP-tagged Cre or ΔCre were used. In case of Lap-tag pulldowns, Brn2, Ascl1, $Myt1l^{FL}$ and $Myt1l^{200–623}$ cDNAs were inserted into Gateway compatible pDONR221 entry vector and inserted into appropriate Gateway destination vectors using LR recombination (Invitrogen). For Flp-In HEK293 stable cell line creation, genes were inserted into pG-LAP6 and pG-LAP7 vectors to generate N- and C-terminally LAP-tagged TFs, respectively.

Tip60 point and deletion mutant constructs: Two approaches were used to disrupt the acetyltransferase activity of Tip60: (i) we substituted two residues that mediate acetyl-CoA binding, Q377 and G380, to E (Q337E/G380E)[52,100], or (ii) mutated the conserved auto-acetylation site, K327 (K327A)[101,102]. To disrupt NR-box motif, which is a domain mediating Tip60's interaction with different classes of nuclear receptors[103,104], we introduced L492A/L493A double mutation. Tip60' zinc finger domain was disrupted by a C263A substitution[105]. Tip60's chromodomain was disrupted by point mutation (Y47A) or deletion of all of the conserved aromatic amino acids that mediate the recognition of methyl groups on modified lysine residues[24,58].

Lentivirus generation and transduction—Lentiviruses were produced in HEK293T cells (ATCC) by co-transfection of three helper plasmids (pRSV-REV, pMDLg/pRRE and VSVG) using polyethyleneimine (PEI)[106]. Only virus preparations with >90% infection efficiency, as assessed by immunofluorescence detecting transgene-positive cells, were used in reprogramming experiments. In general, cells were infected overnight with lentiviral particles in their corresponding growth medium supplemented with 8 μg/ml of polybrene (or 0.5 μg/ml in case of NPCs). sgRNA and shRNA infected cell populations were selected for 1 to 2 days using 2 μg/ml puromycin.

iN cell reprogramming—MEFs were co-infected with rtTA alone[107], or rtTA and the indicated TF-expressing lentiviruses, and reprogramed as previously described[15] (Figure 1A). Briefly, to activate transgene expression MEF medium was supplemented with 2 μg/ml doxycycline (dox) (Sigma) 2 days after infection. The cells were then transferred into N3 medium (DMEM/F12, N2 supplement, 25 μg/ml insulin) containing dox two days later and allowed to reprogram for 14-21 days. The medium was refreshed every 3 days and dox retained in the medium throughout the duration of the experiment.

For RNAi knockdown experiments, the cells were co-transduced with either empty vector control (vector), non-targeting control shRNA (shNTC), or indicated shRNAs. In case of CRISPR/Cas9, sgRNA targeting Renilla sequence was used as a control[50].

To assess reprogramming efficiency of TauGFP MEFs, the cells were dissociated using 0.05% trypsin at days 5 or 7 post-dox and the number of GFP-positive cells was quantified

by FACS. The reprogramming efficiency was then determined as % of TauGFP positive cells, or a relative % of TauGFP, where the fraction of TauGFP was normalized to that of the control. Alternatively, reprograming efficiency was measured as a fraction of TUJ^+ cells with at least one process double the size of the cell body, present in 10 randomly selected 10x fields of view[108]. Counts obtained from three biological replicates were then normalized to the number of neuronal cells in the control. Statistical significance was assessed by one-way or two-way ANOVA, as indicated in figure legends, with post-hoc correction using GraphPad Prism software.

Conversion of inducible Ascl1-expressing v6.5 mESCs into neurons was initiated by induction of Ascl1 expression using dox-containing N3 medium, and the efficiency of reprogramming determined as described above.

Where indicated, the cells were treated with pan-cyclin inhibitor SU9516 (Selleckchem), which causes G1 and G2/M cell cycle blocks[51,56,57].

Myogenic reprogramming—MEFs were co-infected with rtTA, MyoD1 and the indicated shRNAs (Figure S2N). MyoD1 expression was induced using dox 2 days after transduction. After two days the cells were transferred to DMEM/F12 containing 2% horse serum (Thermo Fisher Scientific) and allowed to reprogram for a total of 12 days. Reprogramming efficiency was estimated as a fraction of DES^+ cells.

Inducible CRISPR/Cas9—We used Cas9 fused to the FKBP12-derived destabilizing domain (DD) that enables temporal control of Cas9 expression using the cell-permeable FKBP12 synthetic ligand, Shield-1[50]. In the absence of Shield-1 DD-Cas9 is targeted to the proteasome for degradation, whereas treatment with Shield-1 leads to protein stabilization, thus enabling genomic editing. To deplete Tip60 the cells were infected with EDCPP lentivirus encoding control sgRNA targeting Renilla, or sgRNAs targeting Tip60, selected with puromycin, and Shield-1 (Cheminpharma) was added to the culture medium at given concentrations and for indicated durations.

Differentiation—NPCs constitutively expressing SpCas9-P2A-EGFP were infected with sgRNAs (pLentiGuide) and indicated lentiviruses, and infected cell populations were selected with puromycin. Differentiation was induced 2-3 days after lentiviral transduction by EGF and FGF withdrawal and supplementing the medium with 1% fetal bovine serum (HyClone). Differentiation efficiency was determined as a fraction of TUJ^+ cells present in 10 randomly selected 10x fields of view, relative to the control. Statistical significance was assessed by one-way ANOVA with post-hoc correction using GraphPad Prism software.

Immunocytochemistry and cell counting—Cells were fixed with 4% (wt/vol) paraformaldehyde (USB, 19943) for 10 min at RT. Following fixation, the cells were washed 3X with PBS, permeabilized with PBS containing 0.2% Triton X-100 and blocked for 30 min in PBS containing 0.1% Triton X-100 and 5% CCS. Primary antibodies were diluted in blocking solution and incubated with the fixed cells O/N at 4°C. Cells were washed twice with PBS and incubated with Alexa-conjugated secondary antibodies (1:1000, Invitrogen) in PBS for 1h. Cells were then stained with DAPI for 1min, washed twice with

PBS and imaged using a DM6000 B microscope (Leica). Antibodies used include: MAP2 (1:20,000, Abcam, ab5392), TUJ1 (1:1000, BioLegend, 801202), Desmin (DES, 1:200, Abcam, ab32362), HA.11 (1:1000, BioLegend, 901501), H2A.Zac (Lys4/Lys7, 1:1000, Cell Signaling Technology, #75336), Ki67 (1:1000, BD, 550609). The efficiency of neuronal induction was determined as the number of TUJ1 present in 10 randomly selected 10x fields of view. Counts obtained from three biological replicates were then normalized to the number of neuronal cells in the control.

Annexin V staining—Apoptosis rates were quantified by APC Annexin V/PI staining (BD Biosciences) following the protocol provided by the manufacturer. Briefly, Ascl1 and Brn2/Ascl1/Myt1l infected cells (n=2, biological replicates) were trypsinized at indicated times, washed 2X with cold PBS, and resuspended in 1X binding buffer (10 mM HEPES (pH 7.4), 140 mM NaCl, 2.5 mM $CaCl_2$) at ~1 x 10^6 cells/ml. 100 μl cell aliquots were incubated with Annexin V/PI for 15 min at RT, diluted to 500 μl with binding buffer and Annexin V^+/PI^- population was quantified by flow cytometry.

BrdU incorporation and cell cycle analysis—MEFs were incubated with 10 μM 5-Bromo-2′-deoxyuridine (BrdU, Sigma-Aldrich) for 1h at different times of neuronal induction. The cells were fixed with cold 70% ethanol for 2h and treated with 2N HCl for 20 min at RT. Cells were washed extensively with PBS, incubated in 100 mM sodium borate for 10 min at RT, washed with PBS and stained with APC-conjugated anti-BrdU antibody (BioLegend, # 364114) for 30 min at RT. The cells were subsequently treated with RNase A (Thermo Fisher Scientific), stained with Propidium Iodide (PI) (Invitrogen) and the cell cycle phase distribution was quantified using LSRFortessa™ fluorescence-activated cell analyzer and FlowJo™ software (BD Biosciences).

Western blotting—Cells were washed with PBS and total cell lysates prepared in buffer containing 75 mM Tris-HCl (pH 6.8), 3.8% SDS, 4 M urea, and 20% glycerol. Lysates were sonicated at 10-15 strokes, resolved by SDS-polyacrylamide gel electrophoresis (PAGE) and analyzed by immunoblotting. Primary antibodies used were: HSP90 (Cell Signaling Technology, #4874), TIP60 (Santa Cruz, sc-166323), ASCL1 (Abcam, ab74065), MAP2 (Sigma-Aldrich, M9942), TUJ1 (BioLegend, 801202), FLAG (Sigma-Aldrich, F7425), SIN3B (Santa Cruz, sc-996), HA.11 (mouse, BioLegend, 901501), HA.11 (rabbit, BioLegend, 902301), β-ACTIN (Sigma-Aldrich, A5441), H2Aac (Lys5, Cell Signaling Technology, 2576), H2A.Zac (Lys4/Lys7, Cell Signaling Technology, 75336), H2A (Cell Signaling Technology, 12349), H2A.Z (Active Motif, 39113), H2A.Z (Abcam, ab4174), H3K9ac (Cell Signaling Technology, #9649), H3K14ac (Cell Signaling Technology, #7627), H3K18ac (Cell Signaling Technology, #13998), H3K27ac (Abcam, ab4729), H3K56ac (Cell Signaling Technology, #4243), H3 (Cell Signaling Technology, #3638), H4K5ac (Cell Signaling Technology, #8647), H4K12ac (Cell Signaling Technology, #13944), H4K16ac (Millipore, 07-329), H4 (Cell Signaling Technology, #2935).

Immune complexes were detected using species-specific HRP-conjugated secondary Abs (1:5000, Jackson ImmunoResearch) and enhanced chemiluminescence (Perkin Elmer), or fluorescently labelled IRDye secondary antibodies (1:5000, LI-COR), and subsequently imaged using ChemiDoc imager (BioRad) or near-IR fluorescence scanner (Odyssey

Imaging System, LI-COR). Signal intensities were quantified using Image Lab™ (BioRad) and Image Studio™ (LI-COR) software.

Fluorescence Recovery After Photobleaching (FRAP)—FRAP was performed as described[109]. Briefly, MEFs were plated on glass-bottom 35 mm dishes (MatTek) and infected with lentiviruses expressing the Halo-tagged constructs under a dox-inducible promoter. Two days post-dox the cells were labeled with 100 nM JF-549-HaloTagLigand (a gift from Luke Lavis's lab[110]) for 30 min. The cells were then washed twice with MEF media, followed by one 30 min wash, and two more brief washes, before one final wash in phenol-red-free MEF media that was used during imaging. FRAP was performed on a Zeiss LSM 710 confocal microscope at the Stanford Wu Tsai Neuroscience Microscopy Service, with temperature and CO_2 control, using a 63X oil-immersion objective. Images were acquired with the 561 nM laser at a frequency of 1 Hz. A bleach spot was made using 100% laser power. 10 frames were acquired pre-bleach to get a baseline, and 120 frames were acquired after. Data analysis was performed using MatLab as previously described[111]. The mean FRAP recovery was plotted for each construct and fit using a double-exponential model and logarithmically spaced timepoints.

RNA sequencing

Cell culture conditions and lentiviral transduction: In general, the cells were maintained as described above. Notably, neural induction leads to rapid cell cycle exit in MEFs. Therefore, to compare the effects of Tip60 knockdown between MEFs and Ascl1-transduced MEFs, MEFs were not passaged after reaching confluency, thereby preventing the reactivation of proliferation.

RNA isolation and preparation of RNA-seq libraries: Total RNA was extracted with Trizol (Invitrogen), subjected to DNAse treatment using RQ1 RNAse-free DNAse (Promega) and purified using RNeasy MinElute cleanup kit (Qiagen). For rtTA+shNTC samples and day 2 Ascl1-iN dataset, RNA was reverse-transcribed using Ovation RNA-seq System V2 (NuGEN) and cDNA sheared using Covaris S2 ultrasonicator. Sheared cDNA was subsequently cleaned up with Agencourt AMPure XP beads (Beckman Coulter) and sequencing libraries constructed using NEBNext Ultra DNA Library Prep Kit (New England Biolabs). Library quality and quantity were assessed by Bioanalyzer (Agilent). Paired-end sequencing reads (150bp) were generated on HiSeq4000 (Illumina) at Stanford Functional Genomics Facility (SFGF). For MEF dataset and iN dataset containing 2 biological replicates of day 2 Ascl1+shNTC and all day 5 iN conditions, Poly(A) selected libraries were generated and sequenced on NovaSeq6000 in paired-end mode (150bp) by Novogene.

Differential expression analysis: Raw reads were trimmed for base call quality (PHRED score ≥ 21) using skewer 0.2.2[112] and transcript quantification was performed using mm10 reference transcriptome (GENCODE vM18) and salmon 1.4.0[113]. Count normalization and differential gene expression analysis from two biological replicates were performed using DESeq2 package[114] in R[115] applying adaptive t prior shrinkage estimator 'apeglm'[116]. For comparisons between different batches, the batch effects were estimated using Surrogate Variable Analysis (SVA)[117] and used for differentially expressed gene (DEG) identification

with DESeq2. Unless otherwise indicated, DEGs were identified by selecting genes that changed expression at least 1.5-fold (padj≤0.05). TPM and normalized counts used for visualization were batch adjusted with *limma*[118]. In case of the knockdowns, only DEGs that passed the significance and/or fold change threshold for both Tip60 shRNAs were included for downstream analyses.

The identified DEGs were subjected to fuzzy c-means clustering using Mfuzz v2.44.0 package in R[119] applying c-means parameter of 2.01 to assign genes to 5 clusters summarizing variability between the conditions, and subsequently visualized in R[120].

Gene ontology, GSEA and ISMARA analysis: Gene ontology term enrichment analysis was performed with DAVID 6.8[121] using annotations for GOTERM_BP_FAT.

MEF gene signature was compiled using genes that were enriched at least 15-fold in MEFs when compared to day 7 TauGFP$^+$ Ascl1-iN cells (352 genes, padj≤0.01), as determined based on the analysis of the previously published dataset[16] (Table S4). For GSEA, DEGs between day 5 Ascl1-iN expressing shNTC or those expressing shTip60 were ranked by Wald test statistics and enrichment test was performed using *fgsea*[122]. Gene expression signatures of myocytes, hepatocytes and keratinocytes were generated as described[36], and odds ratio analysis was performed using the *GeneOverlap* (v1.28.0)[123].

TF activity analysis was performed using Integrated System for Motif Activity Response Analysis (ISMARA[65]). ISMARA integrates gene expression data with motif occurrence analysis to predict TF activity profiles, and thus to infer which TFs are most likely driving the expression changes across the samples. The direction of the ISMARA z-score for the identified enriched motifs was determined by multiplying the z-score of a given motif by the sign of Pearson correlation between the predicted TF activity and the expression of its target genes.

Gene classes: Genes induced in MEFs upon Ascl1 expression were grouped based on their expression in the starting MEF population into 1) expressed (‘on’), and 2) not expressed in MEF’s (‘off’), by setting the expression threshold corresponding to FPKM=1 and subsequently selecting genes based on their average FPKM value in rtTA+shNTC condition. The ‘off’ genes were subsequently divided based on the profile of their induction into i) ‘early’, whose expression reaches maximum at day2, and ii) ‘late’, whose expression continues to increase significantly beyond day 2, or which are induced only at day 5 of reprograming. Genes repressed upon Ascl1 induction were classified into i) ‘transient’, showing downregulation at day 2 followed by upregulation at day 5, ii) ‘early’, genes downregulated at day 2 of reprogramming, and iii) ‘late’, genes that are significantly downregulated only at day 5.

Odds ratio analysis was performed using the *GeneOverlap* (v1.28.0)[123], using DEGs sets: i) Ascl1+shNTC vs rtTA+shNTC (fc≥1.5, padj≤0.05), and ii) subset of Ascl1+shNTC vs rtTA+shNTC DEGs that includes Ascl1 targets (see below) significantly affected by Tip60 RNAi (padj≤0.01).

Assay of Transposase-Accessible Chromatin with sequencing (ATAC-seq)

Preparation of ATAC-seq libraries and sequencing: ATAC-seq was performed essentially as previously described[124] following DAPI (Sigma) staining and FACS enrichment for viable cells using FACS-Aria II sorter (BD Biosciences). Sequencing was performed using 2x75bp reads on Illumina NextSeq 500 instrument at SFGF, or 2x150bp on Illumina NovaSeq6000 (Novogene).

ATAC-seq data analysis: Primary data processing, including adapter trimming, genomic alignment to mm10 using Bowtie2 (v 2.3.4.3)[125], mitochondrial reads and duplicate alignment removal, peak calling and reproducibility analysis using MACS2[126] and IDR[127], respectively, were performed using ENCODE ATAC-seq pipeline v1.2.0[128] (https://github.com/ENCODE-DCC/atac-seq-pipeline). Reproducible peaks selected with IDR (idr threshold ≤ 0.05) were aggregated to a final superset of putative regulatory elements that are accessible in at least one of the conditions. The *featureCounts* package was then used to obtain ATAC-seq read counts for each of the regions[129], followed by normalization and differential accessibility analysis using DESeq2. For comparisons involving knockdown conditions, only sites that passed the significance and fold change threshold for both Tip60 shRNAs (or for shH2A.Z#4 and shH2A.Z#5, in case of the analysis of H2A.Z knockdown dataset), were marked as differentially accessible. The identified differentially accessible sites (fc≥2, padj≤0.05) were subjected to fuzzy c-means clustering using Mfuzz.

Open chromatin signatures: Open chromatin signatures for MEF and iN cells were determined by extracting ATAC-seq peaks that are unique for MEFs or for day 5 TauGFP$^+$ Ascl1-iN (fc≥2, padj≤0.05), respectively, based on the analysis of the previously published dataset[16]. Genomic region annotation and gene ontology enrichment were performed using GREAT[130]. Bigwig files were produced using deepTools and reads per genomic content (RPGC) normalization[131], and visualized in R or CiCSC genome browser[132,133].

Cut&Tag

Library preparation and sequencing: The 3XFlag-pA-Tn5-Fl plasmid (Addgene plasmid #124601) was transformed into C3013 cells (NEB), and Tn5 transposase fused to Protein A (pA-Tn5) was purified and loaded with adapters following the previously described protocol[134].

Cells were dissociated using Accutase (Thermo Fisher Scientific) and where indicated, TauGFP$^+$ cell were sorted by FACS. 1x10^5 cells were bound to Concanavalin A beads (Bangs Laboratories) in Wash buffer (20 mM HEPES (pH 7.5), 150 mM NaCl, 0.5 mM Spermidine, complete protease inhibitors (Roche)). Cells were then resuspended in Dig-Wash buffer (Wash buffer containing 0.05% Digitonin) that was additionally supplemented with 0.1% BSA (Sigma) and 2 mM EDTA and subjected to Cut&Tag essentially as described[134]. Briefly, the cells were incubated with 1:50 dilution of primary antibody, or a corresponding control IgG, overnight at 4°C, followed by incubation with guinea pig anti-rabbit IgG (antibodies-online) for 1h at RT. After 3X washes with Dig-Wash buffer the cells were incubated with pA-Tn5 adapter complex prepared in Dig-300 Wash buffer (20 mM HEPES (pH 7.5), 300 mM NaCl, 0.5 mM Spermidine, 0.01% Digitonin, complete

protease inhibitors (Roche)) for 1h at RT. Cells were washed 3X with Dig-300 Wash buffer and subjected to tagmentation in Dig-300 Wash buffer supplemented with 10 mM $MgCl_2$ for 1h at 37°C. To stop tagmentation, the mixture was adjusted to 16.5 mM EDTA and 0.1% SDS and digested with Proteinase K (Thermo Fisher Scientific) overnight at 37°C. Tagmented DNA was purified using phenol-chloroform and the libraries amplified using uniquely barcoded i5/i7 primer pairs (IDT)[124]. Libraries were purified using Agencourt AMPure XP beads (Beckman Coulter), library quality and quantity were assessed by AATI Fragment Analyzer and paired-end sequencing reads (150bp) were generated on Illumina HiSeq4000.

Antibodies used for Cut&Tag were: H2A.Zac (Lys4/Lys7, Cell Signaling Technology, 75336), H2A.Z (Active Motif, 39113), H3K4me3 (Active Motif, 39060), TIP60 (a kind gift of Dr. Bruno Amati, European Institute of Oncology[135]).

Sequence alignment, peak calling and differential enrichment analysis: Reads were trimmed using cutadapt and aligned with Bowtie2 (v 2.3.5.1) to mm10 reference genome. Initial lenient peaks were called with MACS2 (2.2.7.1) with "-p 0.01". For Tip60 Cut&Tag, reproducible peaks were identified using IDR with cutoff idr≤0.1. In case of histone Cut&Tag, MACS2 peaks were called on pooled replicates, and those that were also identified in each of the individual replicates were marked as reproducible. Reproducible peaks were subsequently aggregated using bedtools[136]. *featureCounts* package was used to obtain read counts for each of the regions[129], followed by normalization and differential enrichment analysis using DESeq2. Unless otherwise indicated, DE parameters used were as follow: for histones, fc≥2, padj≤0.05, for Tip60, fc≥2, padj≤0.1.

Bigwig files were produced with deepTools using RPGC normalization and the pooled alignment bam files, with the exception of H2A.Zac Cut&Tag dataset containing Tip60 knockdown conditions, which was normalized to the carry-over *E. coli* DNA that is present in pA-Tn5 prep to account for the global change in H2A.Zac signal[134].

Unless otherwise indicated, co-localization of peak regions was determined based on the overlap of at least 1bp. Average enrichment values were obtained using deepTools and normalized bigwig files by extracting mean scores across genomic ranges of ±250 bp (H2A.Z, Tip60, ATAC-seq) or ±500bp (H3K4me3 and H3K27me3) surrounding TSS or Ascl1 peak summits, as indicated. Heatmaps of Cut&Tag enrichment were generated in R.

Peak classification: For peak classification the criteria used were as follows: promoter: −2kb to +1kb around transcription start site (TSS), enhancer: 2kb to 10kb upstream of TSS, gene body: encompassing exons and introns, gene tail: 2kb downstream of transcription end site (TES), intergenic: none of the above.

DNA motif search: *De novo* motif search within the Tip60 bound regions was performed using peaks that gain enrichment at day 2 of iN induction, as identified by DESeq2 (fc≥2, padj≤0.1) using findMotifsGenome.pl from HOMER v4.11.1[137].

Chromatin State Discovery and Characterization—Hidden Markov Model (ChromHMM): Enrichment and annotation of genomic regions to distinct chromatin states was performed using ChromHMM software (v1.20) as described[138]. Briefly, to generate chromatin state models, histone mark peak files were converted into binarized data, and 15- or 18-state models were generated using *LearnModel* function in ChromHMM. The enrichment for H2A.Z, H2A.Zac and Tip60 for each segment was obtained through *OverlapEnrichment* function and plotted in R, whereas enrichment for TSS regions of Tip60-regulated 'off' genes was visualized using *NeighborhoodEnrichment* function in ChromHMM. Datasets used for ChromHMM analysis were obtained from ENCODE portal (see below), Mikkelsen et al.[69], and H2A.Z and H2A.Zac data used were generated in this study. Gene set enrichment and tissue specificity analysis were performed by Functional Mapping and Annotation (FUMA)[139,140], using genes whose TSS overlap ChromHMM states 7 or 9.

Ascl1 binding sites: Ascl1 chromatin binding in MEFs was determined based on the previously generated ChIP-seq dataset[17]. Briefly, Ascl1 ChIP-seq reads were trimmed using cutadapt and aligned with Bowite2 (v 2.3.5.1) to mm10 reference genome. Initial lenient peaks were called with MACS2 with parameter "-p 0.01", and peak self-consistency was determined with IDR using pseudo-replicate peak calls with cutoff of idr≤0.05. Ascl1 target genes were determined by assigning genes to Ascl1 peaks using GREAT[130] (Table S5). For enhancer/promoter comparisons, Ascl1 binding sites (enhancers) and the nearest TSS were selected, and the normalized enrichment around Ascl1 peak summits or TSS was extracted and visualized as described above.

Publicly Available Data Sets Used: ChIP-seq data obtained from ENCODE portal are: H3K4me1 (ENCSR000CAZ), H3K4me3 (ENCSR000CBA), CTCF (ENCSR000CBW), POLR2A (ENCSR000CBX), H3K27ac (ENCSR000CDI), control (ENCSR000CBB). The GEO accession numbers for the previously published ChIP-seq, ATAC-seq and RNA-seq data are: GSE12241, GSE43916 and GSE101397.

BirA* and FLAG/His^7 pulldowns and mass spectrometry—MEFs were infected with lentiviruses encoding reprogramming factors fused to BirA biotin ligase mutant (R118G, BirA*)[33], BirA* alone or rtTA alone as controls, or with viruses expressing FLAG/His^7 tagged proteins or empty vector control. After 16 – 20h cells were placed in fresh medium containing 2 μg/ml dox to induce transgene expression. For BirA* infected cells the medium was supplemented with 50 μM biotin 24h later and biotinylation allowed to continue for another 24h. At day 3 after infection the cells were harvested by trypsinization, washed twice with ice cold PBS and snap frozen in liquid nitrogen for subsequent affinity purification.

BirA affinity pulldown: For BirA* labeling experiments, 2-4x10^7 cells were lysed in 1 ml of cell lysis buffer (50 mM Tris-HCl (pH 7.5), 0.5% Tween-20, 2 mM EDTA, 1mM DTT, 5mM NaF, 1mM PMSF, complete protease inhibitors (Roche)) for 15 min on ice. Nuclei were separated by centrifugation (1000 x g, 1min, 4°C), resuspended in 0.5 ml of nuclear lysis buffer (500 mM NaCl, 50 mM Tris-HCl (pH 7.5), 0.4% SDS, 5 mM

EDTA, 1 mM DTT, 5 mM NaF, 1 mM PMSF, 5 μg/ml cytochalasin B (Sigma), complete protease inhibitors (Roche), benzonase (Millipore)) and lysed by sonication at RT. Triton X-100 was then added to the final concentration of 2%, lysates were sonicated again and subsequently diluted with equal volume of cold 50 mM Tris-HCl (pH 7.5). After final round of sonication cell debris were cleared by centrifugation (17,000xg, 15min, 4°C) and supernatant was incubated with 0.6 ml of Streptavidin-coated Dynabeads (MyOne Streptavidin C1, Invitrogen) for 2h at 4°C. Beads were collected and washed (8 min each) at RT as follows: 2X with 0.5 ml wash buffer 1 (2% SDS in dH2O), 1X with 1 ml wash buffer 2 (50 mM HEPES (pH 7.5), 0.1% deoxycholate, 1% Triton X-100, 500 mM NaCl, 1 mM EDTA), 1X with 1 ml wash buffer 3 (10 mM Tris-HCl (pH 8.0), 250 mM LiCl, 0.5% NP-40, 0.5% deoxycholate, 1 mM EDTA), and 2X with 1 ml wash buffer 4 (50 mM Tris-HCl (pH 7.5), and 50 mM NaCl). Samples were subjected to tryptic digest and mass spec analysis as described below.

FLAG/His^7 tandem affinity purification: Nuclear extracts were prepared by first resuspending cells in ice cold buffer A (10 mM HEPES (pH 7.9), 10 mM KCl, 0.1 mM dithiothreitol (DTT), 0.1% NP40, 2 mM Na_3VO_4, complete protease inhibitors (Roche)). After 10min incubation on ice nuclei were pelleted by centrifugation, washed in buffer A without NP40 and subsequently lysed in buffer C (20 mM HEPES (pH 7.9), 600 mM NaCl, 25% glycerol, 1% Triton X-100, 50 mM NaF, 2 mM Na_3VO_4, complete protease inhibitors) for 30 min while rotating at 4°C. Lysates were cleared by centrifugation, diluted with equal volume of buffer D (50 mM Tris-HCl (pH 8.0), 1% Triton X-100, 50 mM NaF, 2 mM Na_3VO_4, complete protease inhibitors) and subjected to immunoprecipitation with anti-FLAG M2 affinity resin (Sigma) for 8h at 4°C. Beads were collected by centrifugation and treated with 200U/ml of benzonase in buffer containing 50 mM Tris-HCl (pH 8.0), 150 mM NaCl, 5% glycerol, 50 mM NaF, 2 mM $MgCl_2$, 2 mM Na_3VO_4, complete protease inhibitors) for 20min at RT. Beads were then washed 5X with FLAG wash buffer (50 mM Tris-HCl (pH 8.0), 300 mM NaCl, 1% Triton X-100, 5% glycerol, 50 mM NaF, 2 mM Na_3VO_4, complete protease inhibitors). Beads were then either washed with 100mM ammonium bicarbonate and subjected to on-bead trypsin digest and mass spectrometry (see below), or the immunoprecipitates were eluted by three consecutive rounds of incubation in FLAG wash buffer supplemented with FLAG peptide (0.2 mg/ml) (Sigma-Aldrich) at 30°C, 15 min each. Eluates were pooled together and diluted into 20 volumes of NiNTA buffer (20 mM Tris-HCl (pH 8.0), 300 mM NaCl, 20 mM Imidazole, 0.5% Triton X-100, 50 mM NaF, 10 mM β-mercaptoethanol (BME), complete protease inhibitors) and incubated with Ni-nitrilotriacetic acid (NTA) resin (Qiagen) for 4h 4°C. The beads were washed as follows: 2X with NiNTA buffer, 2X with NiNTA wash buffer A (20 mM Tris-HCl (pH 8.0), 400 mM NaCl, 2M Urea, 20 mM Imidazole, 0.5% Triton X-100, 50 mM NaF, 10 mM BME, complete protease inhibitors), 2X with NiNTA wash buffer B (20 mM Tris-HCl (pH 8.0), 300 mM NaCl, 20 mM Imidazole, 0.05% Triton X-100, 50 mM NaF, 10 mM BME, complete protease inhibitors) and 3X times with 50 mM Tris-HCl (pH 8.0). Immunoprecipitates were eluted with 50mM Tris-HCl (pH 8.0) supplemented with 300 mM imidazole.

Protein digestion, mass spectrometry and data analysis: Each sample was resuspended in 100 mM ammonium bicarbonate buffer, reduced with 5 mM dithiothreitol (DTT) for 1h at 37°C, alkylated with 14 mM iodoacetamide in dark for 1h, and digested with trypsin at enzyme to protein ratio of 1:20 overnight at 37°C. The resulting peptides were subjected to StageTip[141] desalting and resuspended in 0.1% formic acid for the following capillary nanoLC-MS/MS.

Peptides were separated on an in-house made 20 cm reversed phase column (100 μm inner diameter, packed with ReproSil-Pur C18-AQ 3.0 μm resin (Dr. Maisch GmbH)) equipped with a laser-pulled nanoelectrospray emitter tip. Peptides were eluted at a flow rate of 400 nL/min using a two-step linear gradient including 2-25% buffer B in 70 min and 25-40% B in 20 min (buffer A: 0.2% formic acid and 5% DMSO in water; buffer B: 0.2% formic acid and 5% DMSO in acetonitrile) in a the Eksigent ekspert nanoLC-425 system (AB Sciex). Peptides were then analyzed using LTQ Orbitrap Elite mass spectrometer (Thermo Scientific). Data acquisition was executed in data dependent mode with full MS scans acquired in the Orbitrap mass analyzer with a resolution of 60000 and m/z scan range of 340-1600. The top 20 most abundant ions with intensity threshold above 500 counts and charge states 2 and above were selected for fragmentation using collision- induced dissociation (CID) with isolation window of 2 m/z, collision energy of 35%, activation Q of 0.25 and activation time of 5 ms. The CID fragments were analyzed in the ion trap with rapid scan rate. Dynamic exclusion was enabled with repeat count of 1 and exclusion duration of 30 s. The AGC target was set to 1000000 and 5000 for full FTMS scans and ITMSn scans. The maximum injection time was set to 250 s and 100 s for full FTMS scans and ITMSn scans.

All tandem mass spectra were queried against a “target-decoy” sequence database[142] consisting of the mouse proteome Swissprot database (downloaded on Feb 24, 2019) with added common contaminants using SEQUEST[143]. The parent mass error tolerance was set to 10 ppm and the fragment mass error tolerance to 0.6 Da. Enzyme specificity was set to trypsin, oxidation of methionines was set as variable modification and carbamidomethylation of cysteines was set as static modification. High confidence peptide identifications were selected at a 1% false discovery rate and proteins identification were selected at a 5% false discovery rate with the Percolator algorithm[144].

LAP tandem purification and mass spectrometry—To best optimize the LAP purification procedure and minimize the possibility of carryover, cell culture, preparation of extracts and tandem affinity purification were standardized as described[32]. Briefly, stable LAP cell lines were harvested using detergent. Lysates were clarified by centrifugation (43,000 rpm) and subjected to anti-GFP immunoprecipitation. Bound proteins were eluted from antibody beads using TEV protease, recaptured on S-protein agarose (Novagen), and eluted in 2x NuPAGE sample buffer (Invitrogen). Each purified set of interacting proteins was separated on an individual Bolt™ 4-12% Bis-Tris Plus Protein Gels (Invitrogen) and stained with Coomassie brilliant blue. Samples were run into gels for 20-40mm and divided into 20-40x1mm slices. Each excised lane was, reduced, carboxyamidomethylated and digested with trypsin, and mass spectrometry and peptide identification were carried out at the Stanford MS core facility as previously described[145].

Protein network analysis—For each LC/MS experiment spectral counts were transformed into normalized spectral abundance factors. In case of the experiments in MEFs, bait proteins were purified and analyzed alongside the independent negative controls in order to generate background list of proteins that bind non-specifically ('false positive' hits). For FLAG and FLAG/His[7] purifications the controls consisted of immunoprecipitations performed on empty vector control (no-bait) transduced cells. Control streptavidin pulldowns were performed on extracts from rtTA+BirA* transduced cells. In case of LAP purification, a panel of 66 other experiments also conducted in HEK293 cells was used to calculate lognormal probability distributions, and for each of the observed gene product a Z test was conducted against that background distribution. The Benjamini–Hochberg method was used to correct the obtained *P* values, and gene products were accepted below a false discovery rate of 0.12.

To further interrogate functional connections among the candidates, mass spectrometry results were supplemented with known interactions from the BioGRID database[38], and assembled into an interactome map composed of ~800 unique nodes using Cytoscape[39].

Gene ontology (GO) enrichment analysis and network visualization were performed using ClueGO[146], where overrepresented GO Biological Process terms categories (q-value ≤ 0.05) were visualized as nodes clustered into functional modules and interconnected based on the kappa score (>0.4).

qRT-PCR—RNA was isolated using Trizol (Invitrogen) and RNA Clean & Concentrator (Zymo), and subsequently reverse transcribed with Superscript III (Invitrogen). mRNA levels were quantified by real-time PCR assay using Sybr Green (Thermo Fisher Scientific) and the Applied Biosystems 7900HT Fast real-time PCR system. Expression values were expressed as percent of GAPDH or Rn45s using the formula: 2^{-CT}(target mRNA)/2^{-CT}(housekeeping mRNA) × 100. Primers used are listed in Table S6.

In vitro acetylation assay

Protein purification: Tip60 cDNA was subcloned into pGEX-6P-1 bacterial expression vector (GE Healthcare), and GST and GST-Tip60 were expressed and purified from BL21(DE3) *E. coli* strain (Agilent). Briefly, cells were grown at 37°C until optical density (OD) of the culture reached 0.7. Protein expression was induced using 0.2 mM IPTG for 18 h at 12°C. Cell pellets were lysed by sonication in lysis buffer containing 50 mM Tris-HCl (pH 7.5), 300 mM NaCl, 1% TritonX-100, 5% glycerol and protease inhibitors, and cleared lysates were incubated with Glutathione Sepharose 4b (GE Healthcare) overnight at 4°C. GST beads were washed 3X in wash buffer A (50 mM Tris-HCl (pH 7.5), 600 mM NaCl, 1% TritonX-100, 5% glycerol, PMSF), and 2X in wash buffer B (50 mM Tris-HCl (pH 7.5), 300 mM NaCl), and eluted with wash buffer B supplemented with 12.5 mM glutathione (Sigma). Proteins were then dialyzed against wash buffer B containing 20% glycerol and flash frozen at −80°C.

In vitro HAT assay: *In vitro* acetylation was carried out in 20 μl reactions containing 50 mM Tris-HCl (pH 8.0), 10% glycerol, 0.1 mM EDTA, 1 mM DTT, 100 μM acetyl coenzyme A (acetyl-CoA) (Sigma), 200 ng of recombinant histone H2A.Z (Millipore) and 25 ng or 50

ng of GST, or 10 ng, 20 ng or 50 ng of GST-Tip60, for 30 min at 30°C. The reactions were terminated by addition of 4xSDS sample buffer, and analyzed by immunoblotting using anti-TIP60, anti-H2A.Z and anti-H2A.Zac antibodies.

Native chromatin immunoprecipitation—MEFs expressing HA-tagged H2A.Z constructs were trypsinized 48h after infection and washed with PBS. Cells were then washed once in buffer A (20 mM HEPES (pH 7.5), 10 mM KCl, 1.5 mM $MgCl_2$, 10% glycerol, 1 mM DTT, 5 mM sodium butyrate, protease inhibitors), resuspended in buffer A supplemented with 0.2% TritonX-100 and incubated on ice for 10 min. The nuclei were centrifuged at 1300xg, washed once with digestion buffer (10 mM Tris-HCl (pH 7.5), 15 mM NaCl), and then resuspended in digestion buffer supplemented with 2 mM $CaCl_2$. MNase (Thermo Fisher Scientific) was then added at a concentration of $20U/1x10^6$ cells, and the nuclei incubated at 37°C for 30 min. The reaction was stopped by addition of EGTA to a final concentration of 10 mM, and nuclei were subjected to hypotonic lysis in TE buffer (10 mM Tris-HCl (pH 8.0), 1 mM EDTA) for 30 min on ice with occasional mixing. The mixture was then adjusted to 150 mM NaCl by addition of 3x buffer D (60 mM HEPES (pH 7.5), 450 mM NaCl, 4.5 mM $MgCl_2$, 0.6 mM EGTA, 1.5% TritonX-100, 30% glycerol, protease inhibitors), cleared by centrifugation, and clarified supernatant was subjected to immunoprecipitation using anti-HA magnetic beads (Thermo Fisher Scientific) overnight at 4°C. Beads were subsequently washed 5X with buffer D, eluted in 2x SDS sample buffer and analyzed by immunoblotting using anti-HA and anti-H3 antibodies.

QUANTIFICATION AND STATISTICAL ANALYSIS

All data presented summarize results obtained from at least two independent biological replicates. Statistical analyses were performed in R or using GraphPad Prism, as indicated. Statistical details for the individual experiments, including number of replicates (n), significance levels and statistical tests used, have been provided in the main text, figure legends and Methods Details.

Supplementary Material

Refer to Web version on PubMed Central for supplementary material.

Acknowledgements

We thank the Wernig lab members for discussions and Kyle Loh and Cheen Euong Ang for helpful comments on the manuscript. We thank Bruno Amati for Tip60 antibody and Luke Lavis for providing the JF dye. We also thank the Stanford Wu Tsai Neuroscience Microscopy Service. This study was supported by the Howard Hughes Medical Institute Faculty Scholar Award (M.W.), the NIH grant R35GM139569 (O.G.), and the Spectrum Child Health Research Institute at Stanford University (J.A.J.). Some sequencing data were generated on Illumina HiSeq4000 purchased with NIH funds (S10OD018220) (SFGF). Some of the graphics were created with BioRender.com.

References

1. Wang H, Yang Y, Liu J, and Qian L (2021). Direct cell reprogramming: approaches, mechanisms and progress. Nat Rev Mol Cell Biol 22, 410–424. 10.1038/s41580-021-00335-z. [PubMed: 33619373]
2. Deng W, Jacobson EC, Collier AJ, and Plath K (2021). The transcription factor code in iPSC reprogramming. Curr Opin Genet Dev 70, 89–96. 10.1016/j.gde.2021.06.003. [PubMed: 34246082]

3. Hochedlinger K, and Plath K (2009). Epigenetic reprogramming and induced pluripotency. Development 136, 509–523. 10.1242/dev.020867. [PubMed: 19168672]
4. Luna-Zurita L, and Bruneau BG (2013). Chromatin modulators as facilitating factors in cellular reprogramming. Curr Opin Genet Dev 23, 556–561. 10.1016/j.gde.2013.07.002. [PubMed: 23993229]
5. Zaret KS (2020). Pioneer Transcription Factors Initiating Gene Network Changes. Annu Rev Genet 54, 367–385. 10.1146/annurev-genet-030220-015007. [PubMed: 32886547]
6. Hota SK, and Bruneau BG (2016). ATP-dependent chromatin remodeling during mammalian development. Development 143, 2882–2897. 10.1242/dev.128892. [PubMed: 27531948]
7. Bertrand N, Castro DS, and Guillemot F (2002). Proneural genes and the specification of neural cell types. Nat Rev Neurosci 3, 517–530. 10.1038/nrn874. [PubMed: 12094208]
8. Dennis DJ, Han S, and Schuurmans C (2019). bHLH transcription factors in neural development, disease, and reprogramming. Brain Res 1705, 48–65. 10.1016/j.brainres.2018.03.013. [PubMed: 29544733]
9. Guillemot F, Lo LC, Johnson JE, Auerbach A, Anderson DJ, and Joyner AL (1993). Mammalian achaete-scute homolog 1 is required for the early development of olfactory and autonomic neurons. Cell 75, 463–476. 10.1016/0092-8674(93)90381-y. [PubMed: 8221886]
10. Lo LC, Johnson JE, Wuenschell CW, Saito T, and Anderson DJ (1991). Mammalian achaete-scute homolog 1 is transiently expressed by spatially restricted subsets of early neuroepithelial and neural crest cells. Genes Dev 5, 1524–1537. 10.1101/gad.5.9.1524. [PubMed: 1909283]
11. Ma Q, Fode C, Guillemot F, and Anderson DJ (1999). Neurogenin1 and neurogenin2 control two distinct waves of neurogenesis in developing dorsal root ganglia. Genes Dev 13, 1717–1728. 10.1101/gad.13.13.1717. [PubMed: 10398684]
12. Nakada Y, Hunsaker TL, Henke RM, and Johnson JE (2004). Distinct domains within Mash1 and Math1 are required for function in neuronal differentiation versus neuronal cell-type specification. Development 131, 1319–1330. 10.1242/dev.01008. [PubMed: 14993186]
13. Kageyama R, Shimojo H, and Ohtsuka T (2019). Dynamic control of neural stem cells by bHLH factors. Neurosci Res 138, 12–18. 10.1016/j.neures.2018.09.005. [PubMed: 30227160]
14. Chanda S, Ang CE, Davila J, Pak C, Mall M, Lee QY, Ahlenius H, Jung SW, Sudhof TC, and Wernig M (2014). Generation of induced neuronal cells by the single reprogramming factor ASCL1. Stem Cell Reports 3, 282–296. 10.1016/j.stemcr.2014.05.020. [PubMed: 25254342]
15. Vierbuchen T, Ostermeier A, Pang ZP, Kokubu Y, Sudhof TC, and Wernig M (2010). Direct conversion of fibroblasts to functional neurons by defined factors. Nature 463, 1035–1041. 10.1038/nature08797. [PubMed: 20107439]
16. Wapinski OL, Lee QY, Chen AC, Li R, Corces MR, Ang CE, Treutlein B, Xiang C, Baubet V, Suchy FP, et al. (2017). Rapid Chromatin Switch in the Direct Reprogramming of Fibroblasts to Neurons. Cell Rep 20, 3236–3247. 10.1016/j.celrep.2017.09.011. [PubMed: 28954238]
17. Wapinski OL, Vierbuchen T, Qu K, Lee QY, Chanda S, Fuentes DR, Giresi PG, Ng YH, Marro S, Neff NF, et al. (2013). Hierarchical mechanisms for direct reprogramming of fibroblasts to neurons. Cell 155, 621–635. 10.1016/j.cell.2013.09.028. [PubMed: 24243019]
18. Colino-Sanguino Y, Clark SJ, and Valdes-Mora F (2021). The H2A.Z-nuclesome code in mammals: emerging functions. Trends Genet. 10.1016/j.tig.2021.10.003.
19. Giaimo BD, Ferrante F, Herchenrother A, Hake SB, and Borggrefe T (2019). The histone variant H2A.Z in gene regulation. Epigenetics Chromatin 12, 37. 10.1186/s13072-019-0274-9. [PubMed: 31200754]
20. Keogh MC, Mennella TA, Sawa C, Berthelet S, Krogan NJ, Wolek A, Podolny V, Carpenter LR, Greenblatt JF, Baetz K, et al. (2006). The Saccharomyces cerevisiae histone H2A variant Htz1 is acetylated by NuA4. Genes Dev 20, 660–665. 10.1101/gad.1388106. [PubMed: 16543219]
21. Millar CB, Xu F, Zhang K, and Grunstein M (2006). Acetylation of H2AZ Lys 14 is associated with genome-wide gene activity in yeast. Genes Dev 20, 711–722. 10.1101/gad.1395506. [PubMed: 16543223]
22. Acharya D, Hainer SJ, Yoon Y, Wang F, Bach I, Rivera-Perez JA, and Fazzio TG (2017). KAT-Independent Gene Regulation by Tip60 Promotes ESC Self-Renewal but Not Pluripotency. Cell Rep 19, 671–679. 10.1016/j.celrep.2017.04.001. [PubMed: 28445719]

23. Humbert J, Salian S, Makrythanasis P, Lemire G, Rousseau J, Ehresmann S, Garcia T, Alasiri R, Bottani A, Hanquinet S, et al. (2020). De Novo KAT5 Variants Cause a Syndrome with Recognizable Facial Dysmorphisms, Cerebellar Atrophy, Sleep Disturbance, and Epilepsy. Am J Hum Genet 107, 564–574. 10.1016/j.ajhg.2020.08.002. [PubMed: 32822602]
24. Jeong KW, Kim K, Situ AJ, Ulmer TS, An W, and Stallcup MR (2011). Recognition of enhancer element-specific histone methylation by TIP60 in transcriptional activation. Nat Struct Mol Biol 18, 1358–1365. 10.1038/nsmb.2153. [PubMed: 22081016]
25. Panikker P, Xu SJ, Zhang H, Sarthi J, Beaver M, Sheth A, Akhter S, and Elefant F (2018). Restoring Tip60 HAT/HDAC2 Balance in the Neurodegenerative Brain Relieves Epigenetic Transcriptional Repression and Reinstates Cognition. J Neurosci 38, 4569–4583. 10.1523/JNEUROSCI.2840-17.2018. [PubMed: 29654189]
26. Urban I, Kerimoglu C, Sakib MS, Wang H, Benito E, Thaller C, Zhou X, Yan J, Fischer A, and Eichele G (2019). TIP60/KAT5 is required for neuronal viability in hippocampal CA1. Sci Rep 9, 16173. 10.1038/s41598-019-50927-1. [PubMed: 31700011]
27. Wee CL, Teo S, Oey NE, Wright GD, VanDongen HM, and VanDongen AM (2014). Nuclear Arc Interacts with the Histone Acetyltransferase Tip60 to Modify H4K12 Acetylation(1,2,3). eNeuro 1. 10.1523/ENEURO.0019-14.2014.
28. Colino-Sanguino Y, Cornett EM, Moulder D, Smith GC, Hrit J, Cordeiro-Spinetti E, Vaughan RM, Krajewski K, Rothbart SB, Clark SJ, et al. (2019). A Read/Write Mechanism Connects p300 Bromodomain Function to H2A.Z Acetylation. iScience 21, 773–788. 10.1016/j.isci.2019.10.053. [PubMed: 31727574]
29. Dalvai M, Bellucci L, Fleury L, Lavigne AC, Moutahir F, and Bystricky K (2013). H2A.Z-dependent crosstalk between enhancer and promoter regulates cyclin D1 expression. Oncogene 32, 4243–4251. 10.1038/onc.2012.442. [PubMed: 23108396]
30. Giaimo BD, Ferrante F, Vallejo DM, Hein K, Gutierrez-Perez I, Nist A, Stiewe T, Mittler G, Herold S, Zimmermann T, et al. (2018). Histone variant H2A.Z deposition and acetylation directs the canonical Notch signaling response. Nucleic Acids Res 46, 8197–8215. 10.1093/nar/gky551. [PubMed: 29986055]
31. Yamagata K, Shino M, Aikawa Y, Fujita S, and Kitabayashi I (2021). Tip60 activates Hoxa9 and Meis1 expression through acetylation of H2A.Z, promoting MLL-AF10 and MLL-ENL acute myeloid leukemia. Leukemia. 10.1038/s41375-021-01244-y.
32. Torres JZ, Miller JJ, and Jackson PK (2009). High-throughput generation of tagged stable cell lines for proteomic analysis. Proteomics 9, 2888–2891. 10.1002/pmic.200800873. [PubMed: 19405035]
33. Roux KJ, Kim DI, Raida M, and Burke B (2012). A promiscuous biotin ligase fusion protein identifies proximal and interacting proteins in mammalian cells. J Cell Biol 196, 801–810. 10.1083/jcb.201112098. [PubMed: 22412018]
34. Gillotin S, Davies JD, and Philpott A (2018). Subcellular localisation modulates ubiquitylation and degradation of Ascl1. Sci Rep 8, 4625. 10.1038/s41598-018-23056-4. [PubMed: 29545540]
35. Urban N, van den Berg DL, Forget A, Andersen J, Demmers JA, Hunt C, Ayrault O, and Guillemot F (2016). Return to quiescence of mouse neural stem cells by degradation of a proactivation protein. Science 353, 292–295. 10.1126/science.aaf4802. [PubMed: 27418510]
36. Mall M, Kareta MS, Chanda S, Ahlenius H, Perotti N, Zhou B, Grieder SD, Ge X, Drake S, Euong Ang C, et al. (2017). Myt1l safeguards neuronal identity by actively repressing many non-neuronal fates. Nature 544, 245–249. 10.1038/nature21722. [PubMed: 28379941]
37. Zhang X, Sun F, Qiao Y, Zheng W, Liu Y, Chen Y, Wu Q, Liu X, Zhu G, Chen Y, et al. (2017). TFCP2 Is Required for YAP-Dependent Transcription to Stimulate Liver Malignancy. Cell Rep 21, 1227–1239. 10.1016/j.celrep.2017.10.017. [PubMed: 29091762]
38. Oughtred R, Stark C, Breitkreutz BJ, Rust J, Boucher L, Chang C, Kolas N, O'Donnell L, Leung G, McAdam R, et al. (2019). The BioGRID interaction database: 2019 update. Nucleic Acids Res 47, D529–D541. 10.1093/nar/gky1079. [PubMed: 30476227]
39. Shannon P, Markiel A, Ozier O, Baliga NS, Wang JT, Ramage D, Amin N, Schwikowski B, and Ideker T (2003). Cytoscape: a software environment for integrated models of biomolecular interaction networks. Genome Res 13, 2498–2504. 10.1101/gr.1239303. [PubMed: 14597658]

40. Gupta A, Guerin-Peyrou TG, Sharma GG, Park C, Agarwal M, Ganju RK, Pandita S, Choi K, Sukumar S, Pandita RK, et al. (2008). The mammalian ortholog of Drosophila MOF that acetylates histone H4 lysine 16 is essential for embryogenesis and oncogenesis. Mol Cell Biol 28, 397–409. 10.1128/MCB.01045-07. [PubMed: 17967868]
41. Hu Y, Fisher JB, Koprowski S, McAllister D, Kim MS, and Lough J (2009). Homozygous disruption of the Tip60 gene causes early embryonic lethality. Dev Dyn 238, 2912–2921. 10.1002/dvdy.22110. [PubMed: 19842187]
42. Kueh AJ, Dixon MP, Voss AK, and Thomas T (2011). HBO1 is required for H3K14 acetylation and normal transcriptional activity during embryonic development. Mol Cell Biol 31, 845–860. 10.1128/MCB.00159-10. [PubMed: 21149574]
43. Sapountzi V, and Cote J (2011). MYST-family histone acetyltransferases: beyond chromatin. Cell Mol Life Sci 68, 1147–1156. 10.1007/s00018-010-0599-9. [PubMed: 21132344]
44. Stilling RM, Ronicke R, Benito E, Urbanke H, Capece V, Burkhardt S, Bahari-Javan S, Barth J, Sananbenesi F, Schutz AL, et al. (2014). K-Lysine acetyltransferase 2a regulates a hippocampal gene expression network linked to memory formation. EMBO J 33, 1912–1927. 10.15252/embj.201487870. [PubMed: 25024434]
45. Thomas T, Dixon MP, Kueh AJ, and Voss AK (2008). Mof (MYST1 or KAT8) is essential for progression of embryonic development past the blastocyst stage and required for normal chromatin architecture. Mol Cell Biol 28, 5093–5105. 10.1128/MCB.02202-07. [PubMed: 18541669]
46. Xu S, Wilf R, Menon T, Panikker P, Sarthi J, and Elefant F (2014). Epigenetic control of learning and memory in Drosophila by Tip60 HAT action. Genetics 198, 1571–1586. 10.1534/genetics.114.171660. [PubMed: 25326235]
47. Li L, Ghorbani M, Weisz-Hubshman M, Rousseau J, Thiffault I, Schnur RE, Breen C, Oegema R, Weiss MM, Waisfisz Q, et al. (2020). Lysine acetyltransferase 8 is involved in cerebral development and syndromic intellectual disability. J Clin Invest 130, 1431–1445. 10.1172/JCI131145. [PubMed: 31794431]
48. Treutlein B, Lee QY, Camp JG, Mall M, Koh W, Shariati SA, Sim S, Neff NF, Skotheim JM, Wernig M, et al. (2016). Dissecting direct reprogramming from fibroblast to neuron using single-cell RNA-seq. Nature 534, 391–395. 10.1038/nature18323. [PubMed: 27281220]
49. Zhang Y, Pak C, Han Y, Ahlenius H, Zhang Z, Chanda S, Marro S, Patzke C, Acuna C, Covy J, et al. (2013). Rapid single-step induction of functional neurons from human pluripotent stem cells. Neuron 78, 785–798. 10.1016/j.neuron.2013.05.029. [PubMed: 23764284]
50. Senturk S, Shirole NH, Nowak DG, Corbo V, Pal D, Vaughan A, Tuveson DA, Trotman LC, Kinney JB, and Sordella R (2017). Rapid and tunable method to temporally control gene editing based on conditional Cas9 stabilization. Nat Commun 8, 14370. 10.1038/ncomms14370. [PubMed: 28224990]
51. Acharya D, Nera B, Milstone ZJ, Bourke L, Yoon Y, Rivera-Perez JA, Trivedi CM, and Fazzio TG (2018). TIP55, a splice isoform of the KAT5 acetyltransferase, is essential for developmental gene regulation and organogenesis. Sci Rep 8, 14908. 10.1038/s41598-018-33213-4. [PubMed: 30297694]
52. Ikura T, Ogryzko VV, Grigoriev M, Groisman R, Wang J, Horikoshi M, Scully R, Qin J, and Nakatani Y (2000). Involvement of the TIP60 histone acetylase complex in DNA repair and apoptosis. Cell 102, 463–473. 10.1016/s0092-8674(00)00051-9. [PubMed: 10966108]
53. Squatrito M, Gorrini C, and Amati B (2006). Tip60 in DNA damage response and growth control: many tricks in one HAT. Trends Cell Biol 16, 433–442. 10.1016/j.tcb.2006.07.007. [PubMed: 16904321]
54. Tang Y, Luo J, Zhang W, and Gu W (2006). Tip60-dependent acetylation of p53 modulates the decision between cell-cycle arrest and apoptosis. Mol Cell 24, 827–839. 10.1016/j.molcel.2006.11.021. [PubMed: 17189186]
55. Wichmann J, Pitt C, Eccles S, Garnham AL, Li-Wai-Suen CSN, May R, Allan E, Wilcox S, Herold MJ, Smyth GK, et al. (2022). Loss of TIP60 (KAT5) abolishes H2AZ lysine 7 acetylation and causes p53, INK4A, and ARF-independent cell cycle arrest. Cell Death Dis 13, 627. 10.1038/s41419-022-05055-6. [PubMed: 35853868]

56. Jorda R, Hendrychova D, Voller J, Reznickova E, Gucky T, and Krystof V (2018). How Selective Are Pharmacological Inhibitors of Cell-Cycle-Regulating Cyclin-Dependent Kinases? J Med Chem 61, 9105–9120. 10.1021/acs.jmedchem.8b00049. [PubMed: 30234987]
57. Lane ME, Yu B, Rice A, Lipson KE, Liang C, Sun L, Tang C, McMahon G, Pestell RG, and Wadler S (2001). A novel cdk2-selective inhibitor, SU9516, induces apoptosis in colon carcinoma cells. Cancer Res 61, 6170–6177. [PubMed: 11507069]
58. Sun Y, Jiang X, Xu Y, Ayrapetov MK, Moreau LA, Whetstine JR, and Price BD (2009). Histone H3 methylation links DNA damage detection to activation of the tumour suppressor Tip60. Nat Cell Biol 11, 1376–1382. 10.1038/ncb1982. [PubMed: 19783983]
59. Altaf M, Auger A, Monnet-Saksouk J, Brodeur J, Piquet S, Cramet M, Bouchard N, Lacoste N, Utley RT, Gaudreau L, et al. (2010). NuA4-dependent acetylation of nucleosomal histones H4 and H2A directly stimulates incorporation of H2A.Z by the SWR1 complex. J Biol Chem 285, 15966–15977. 10.1074/jbc.M110.117069. [PubMed: 20332092]
60. Li Z, and Rasmussen LJ (2020). TIP60 in aging and neurodegeneration. Ageing Res Rev 64, 101195. 10.1016/j.arr.2020.101195. [PubMed: 33091598]
61. Pradhan SK, Su T, Yen L, Jacquet K, Huang C, Cote J, Kurdistani SK, and Carey MF (2016). EP400 Deposits H3.3 into Promoters and Enhancers during Gene Activation. Mol Cell 61, 27–38. 10.1016/j.molcel.2015.10.039. [PubMed: 26669263]
62. Ku M, Jaffe JD, Koche RP, Rheinbay E, Endoh M, Koseki H, Carr SA, and Bernstein BE (2012). H2A.Z landscapes and dual modifications in pluripotent and multipotent stem cells underlie complex genome regulatory functions. Genome Biol 13, R85. 10.1186/gb-2012-13-10-r85. [PubMed: 23034477]
63. Semer M, Bidon B, Larnicol A, Caliskan G, Catez P, Egly JM, Coin F, and Le May N (2019). DNA repair complex licenses acetylation of H2A.Z.1 by KAT2A during transcription. Nat Chem Biol 15, 992–1000. 10.1038/s41589-019-0354-y. [PubMed: 31527837]
64. Hsu CC, Shi J, Yuan C, Zhao D, Jiang S, Lyu J, Wang X, Li H, Wen H, Li W, et al. (2018). Recognition of histone acetylation by the GAS41 YEATS domain promotes H2A.Z deposition in non-small cell lung cancer. Genes Dev 32, 58–69. 10.1101/gad.303784.117. [PubMed: 29437725]
65. Balwierz PJ, Pachkov M, Arnold P, Gruber AJ, Zavolan M, and van Nimwegen E (2014). ISMARA: automated modeling of genomic signals as a democracy of regulatory motifs. Genome Res 24, 869–884. 10.1101/gr.169508.113. [PubMed: 24515121]
66. Schoenherr CJ, and Anderson DJ (1995). The neuron-restrictive silencer factor (NRSF): a coordinate repressor of multiple neuron-specific genes. Science 267, 1360–1363. 10.1126/science.7871435. [PubMed: 7871435]
67. Belotti E, Lacoste N, Simonet T, Papin C, Padmanabhan K, Scionti I, Gangloff YG, Ramos L, Dalkara D, Hamiche A, et al. (2020). H2A.Z is dispensable for both basal and activated transcription in post-mitotic mouse muscles. Nucleic Acids Res 48, 4601–4613. 10.1093/nar/gkaa157. [PubMed: 32266374]
68. Blanco E, Gonzalez-Ramirez M, Alcaine-Colet A, Aranda S, and Di Croce L (2020). The Bivalent Genome: Characterization, Structure, and Regulation. Trends Genet 36, 118–131. 10.1016/j.tig.2019.11.004. [PubMed: 31818514]
69. Mikkelsen TS, Ku M, Jaffe DB, Issac B, Lieberman E, Giannoukos G, Alvarez P, Brockman W, Kim TK, Koche RP, et al. (2007). Genome-wide maps of chromatin state in pluripotent and lineage-committed cells. Nature 448, 553–560. 10.1038/nature06008. [PubMed: 17603471]
70. Zhou VW, Goren A, and Bernstein BE (2011). Charting histone modifications and the functional organization of mammalian genomes. Nat Rev Genet 12, 7–18. 10.1038/nrg2905. [PubMed: 21116306]
71. Dunican DS, Mjoseng HK, Duthie L, Flyamer IM, Bickmore WA, and Meehan RR (2020). Bivalent promoter hypermethylation in cancer is linked to the H327me3/H3K4me3 ratio in embryonic stem cells. BMC Biol 18, 25. 10.1186/s12915-020-0752-3. [PubMed: 32131813]
72. Papp B, and Plath K (2013). Epigenetics of reprogramming to induced pluripotency. Cell 152, 1324–1343. 10.1016/j.cell.2013.02.043. [PubMed: 23498940]
73. Sapountzi V, Logan IR, and Robson CN (2006). Cellular functions of TIP60. Int J Biochem Cell Biol 38, 1496–1509. 10.1016/j.biocel.2006.03.003. [PubMed: 16698308]

74. Xiao Y, Nagai Y, Deng G, Ohtani T, Zhu Z, Zhou Z, Zhang H, Ji MQ, Lough JW, Samanta A, et al. (2014). Dynamic interactions between TIP60 and p300 regulate FOXP3 function through a structural switch defined by a single lysine on TIP60. Cell Rep 7, 1471–1480. 10.1016/j.celrep.2014.04.021. [PubMed: 24835996]
75. Wang Z, Zang C, Cui K, Schones DE, Barski A, Peng W, and Zhao K (2009). Genome-wide mapping of HATs and HDACs reveals distinct functions in active and inactive genes. Cell 138, 1019–1031. 10.1016/j.cell.2009.06.049. [PubMed: 19698979]
76. Sankar A, Mohammad F, Sundaramurthy AK, Wang H, Lerdrup M, Tatar T, and Helin K (2022). Histone editing elucidates the functional roles of H3K27 methylation and acetylation in mammals. Nat Genet 54, 754–760. 10.1038/s41588-022-01091-2. [PubMed: 35668298]
77. Bernstein BE, Mikkelsen TS, Xie X, Kamal M, Huebert DJ, Cuff J, Fry B, Meissner A, Wernig M, Plath K, et al. (2006). A bivalent chromatin structure marks key developmental genes in embryonic stem cells. Cell 125, 315–326. 10.1016/j.cell.2006.02.041. [PubMed: 16630819]
78. Voigt P, Tee WW, and Reinberg D (2013). A double take on bivalent promoters. Genes Dev 27, 1318–1338. 10.1101/gad.219626.113. [PubMed: 23788621]
79. Barski A, Cuddapah S, Cui K, Roh TY, Schones DE, Wang Z, Wei G, Chepelev I, and Zhao K (2007). High-resolution profiling of histone methylations in the human genome. Cell 129, 823–837. 10.1016/j.cell.2007.05.009. [PubMed: 17512414]
80. Cui K, Zang C, Roh TY, Schones DE, Childs RW, Peng W, and Zhao K (2009). Chromatin signatures in multipotent human hematopoietic stem cells indicate the fate of bivalent genes during differentiation. Cell Stem Cell 4, 80–93. 10.1016/j.stem.2008.11.011. [PubMed: 19128795]
81. Rada-Iglesias A, Bajpai R, Prescott S, Brugmann SA, Swigut T, and Wysocka J (2012). Epigenomic annotation of enhancers predicts transcriptional regulators of human neural crest. Cell Stem Cell 11, 633–648. 10.1016/j.stem.2012.07.006. [PubMed: 22981823]
82. Roh TY, Cuddapah S, Cui K, and Zhao K (2006). The genomic landscape of histone modifications in human T cells. Proc Natl Acad Sci U S A 103, 15782–15787. 10.1073/pnas.0607617103. [PubMed: 17043231]
83. Sodersten E, Toskas K, Rraklli V, Tiklova K, Bjorklund AK, Ringner M, Perlmann T, and Holmberg J (2018). A comprehensive map coupling histone modifications with gene regulation in adult dopaminergic and serotonergic neurons. Nat Commun 9, 1226. 10.1038/s41467-018-03538-9. [PubMed: 29581424]
84. Douillet D, Sze CC, Ryan C, Piunti A, Shah AP, Ugarenko M, Marshall SA, Rendleman EJ, Zha D, Helmin KA, et al. (2020). Uncoupling histone H3K4 trimethylation from developmental gene expression via an equilibrium of COMPASS, Polycomb and DNA methylation. Nat Genet 52, 615–625. 10.1038/s41588-020-0618-1. [PubMed: 32393859]
85. Kumar D, Cinghu S, Oldfield AJ, Yang P, and Jothi R (2021). Decoding the function of bivalent chromatin in development and cancer. Genome Res. 10.1101/gr.275736.121.
86. Ooi SK, Qiu C, Bernstein E, Li K, Jia D, Yang Z, Erdjument-Bromage H, Tempst P, Lin SP, Allis CD, et al. (2007). DNMT3L connects unmethylated lysine 4 of histone H3 to de novo methylation of DNA. Nature 448, 714–717. 10.1038/nature05987. [PubMed: 17687327]
87. Hu D, Garruss AS, Gao X, Morgan MA, Cook M, Smith ER, and Shilatifard A (2013). The Mll2 branch of the COMPASS family regulates bivalent promoters in mouse embryonic stem cells. Nat Struct Mol Biol 20, 1093–1097. 10.1038/nsmb.2653. [PubMed: 23934151]
88. Shen E, Shulha H, Weng Z, and Akbarian S (2014). Regulation of histone H3K4 methylation in brain development and disease. Philos Trans R Soc Lond B Biol Sci 369. 10.1098/rstb.2013.0514.
89. Vallianatos CN, and Iwase S (2015). Disrupted intricacy of histone H3K4 methylation in neurodevelopmental disorders. Epigenomics 7, 503–519. 10.2217/epi.15.1. [PubMed: 26077434]
90. Fazzio TG, Huff JT, and Panning B (2008). An RNAi screen of chromatin proteins identifies Tip60-p400 as a regulator of embryonic stem cell identity. Cell 134, 162–174. 10.1016/j.cell.2008.05.031. [PubMed: 18614019]
91. Kim JW, Jang SM, Kim CH, An JH, Kang EJ, and Choi KH (2011). Tip60 regulates myoblast differentiation by enhancing the transcriptional activity of MyoD via their physical interactions. FEBS J 278, 4394–1404. 10.1111/j.1742-4658.2011.08362.x. [PubMed: 21936881]

92. van Beekum O, Brenkman AB, Grontved L, Hamers N, van den Broek NJ, Berger R, Mandrup S, and Kalkhoven E (2008). The adipogenic acetyltransferase Tip60 targets activation function 1 of peroxisome proliferator-activated receptor gamma. Endocrinology 149, 1840–1849. 10.1210/en.2007-0977. [PubMed: 18096664]

93. UniProt https://www.uniprot.org/.

94. Tucker KL, Meyer M, and Barde YA (2001). Neurotrophins are required for nerve growth during development. Nat Neurosci 4, 29–37. 10.1038/82868. [PubMed: 11135642]

95. Rideout WM 3rd, Wakayama T, Wutz A, Eggan K, Jackson-Grusby L, Dausman J, Yanagimachi R, and Jaenisch R (2000). Generation of mice from wild-type and targeted ES cells by nuclear cloning. Nat Genet 24, 109–110. 10.1038/72753. [PubMed: 10655052]

96. Ng YH, Chanda S, Janas JA, Yang N, Kokubu Y, Südhof TC, and Wernig M (2021). Efficient generation of dopaminergic induced neuronal cells with midbrain characteristics. Stem Cell Reports 16, 1763–1776. 10.1016/j.stemcr.2021.05.017. [PubMed: 34171286]

97. Sang L, Miller JJ, Corbit KC, Giles RH, Brauer MJ, Otto EA, Baye LM, Wen X, Scales SJ, Kwong M, et al. (2011). Mapping the NPHP-JBTS-MKS protein network reveals ciliopathy disease genes and pathways. Cell 145, 513–528. 10.1016/j.cell.2011.04.019. [PubMed: 21565611]

98. Lee QY, Mall M, Chanda S, Zhou B, Sharma KS, Schaukowitch K, Adrian-Segarra JM, Grieder SD, Kareta MS, Wapinski OL, et al. (2020). Pro-neuronal activity of Myod1 due to promiscuous binding to neuronal genes. Nat Cell Biol 22, 401–411. 10.1038/s41556-020-0490-3. [PubMed: 32231311]

99. Rubin AJ, Parker KR, Satpathy AT, Qi Y, Wu B, Ong AJ, Mumbach MR, Ji AL, Kim DS, Cho SW, et al. (2019). Coupled Single-Cell CRISPR Screening and Epigenomic Profiling Reveals Causal Gene Regulatory Networks. Cell 176, 361–376 e17. 10.1016/j.cell.2018.11.022. [PubMed: 30580963]

100. Wolf E, Vassilev A, Makino Y, Sali A, Nakatani Y, and Burley SK (1998). Crystal structure of a GCN5-related N-acetyltransferase: Serratia marcescens aminoglycoside 3-N-acetyltransferase. Cell 94, 439–449. 10.1016/s0092-8674(00)81585-8. [PubMed: 9727487]

101. Yang C, Wu J, and Zheng YG (2012). Function of the active site lysine autoacetylation in Tip60 catalysis. PLoS One 7, e32886. 10.1371/journal.pone.0032886. [PubMed: 22470428]

102. Yuan H, Rossetto D, Mellert H, Dang W, Srinivasan M, Johnson J, Hodawadekar S, Ding EC, Speicher K, Abshiru N, et al. (2012). MYST protein acetyltransferase activity requires active site lysine autoacetylation. EMBO J 31, 58–70. 10.1038/emboj.2011.382. [PubMed: 22020126]

103. Bakshi K, Ranjitha B, Dubey S, Jagannadham J, Jaiswal B, and Gupta A (2017). Novel complex of HAT protein TIP60 and nuclear receptor PXR promotes cell migration and adhesion. Sci Rep 7, 3635. 10.1038/s41598-017-03783-w. [PubMed: 28623334]

104. Gaughan L, Brady ME, Cook S, Neal DE, and Robson CN (2001). Tip60 is a co-activator specific for class I nuclear hormone receptors. J Biol Chem 276, 46841–46848. 10.1074/jbc.M103710200. [PubMed: 11591700]

105. Nordentoft I, and Jorgensen P (2003). The acetyltransferase 60 kDa trans-acting regulatory protein of HIV type 1-interacting protein (Tip60) interacts with the translocation E26 transforming-specific leukaemia gene (TEL) and functions as a transcriptional co-repressor. Biochem J 374, 165–173. 10.1042/BJ20030087. [PubMed: 12737628]

106. Longo PA, Kavran JM, Kim MS, and Leahy DJ (2013). Transient mammalian cell transfection with polyethylenimine (PEI). Methods Enzymol 529, 227–240. 10.1016/B978-0-12-418687-3.00018-5. [PubMed: 24011049]

107. Hockemeyer D, Soldner F, Cook EG, Gao Q, Mitalipova M, and Jaenisch R (2008). A drug-inducible system for direct reprogramming of human somatic cells to pluripotency. Cell Stem Cell 3, 346–353. 10.1016/j.stem.2008.08.014. [PubMed: 18786421]

108. Schindelin J, Arganda-Carreras I, Frise E, Kaynig V, Longair M, Pietzsch T, Preibisch S, Rueden C, Saalfeld S, Schmid B, et al. (2012). Fiji: an open-source platform for biological-image analysis. Nat Methods 9, 676–682. 10.1038/nmeth.2019. [PubMed: 22743772]

109. Teves SS, An L, Hansen AS, Xie L, Darzacq X, and Tjian R (2016). A dynamic mode of mitotic bookmarking by transcription factors. Elife 5. 10.7554/eLife.22280.

110. Grimm JB, English BP, Chen J, Slaughter JP, Zhang Z, Revyakin A, Patel R, Macklin JJ, Normanno D, Singer RH, et al. (2015). A general method to improve fluorophores for live-cell and single-molecule microscopy. Nat Methods 12, 244–250, 3 p following 250. 10.1038/nmeth.3256. [PubMed: 25599551]
111. Hansen AS, Pustova I, Cattoglio C, Tjian R, and Darzacq X (2017). CTCF and cohesin regulate chromatin loop stability with distinct dynamics. Elife 6. 10.7554/eLife.25776.
112. Jiang H, Lei R, Ding SW, and Zhu S (2014). Skewer: a fast and accurate adapter trimmer for next-generation sequencing paired-end reads. BMC Bioinformatics 15, 182. 10.1186/1471-2105-15-182. [PubMed: 24925680]
113. Patro R, Duggal G, Love MI, Irizarry RA, and Kingsford C (2017). Salmon provides fast and bias-aware quantification of transcript expression. Nat Methods 14, 417–419. 10.1038/nmeth.4197. [PubMed: 28263959]
114. Love MI, Huber W, and Anders S (2014). Moderated estimation of fold change and dispersion for RNA-seq data with DESeq2. Genome Biol 15, 550. 10.1186/s13059-014-0550-8. [PubMed: 25516281]
115. RCoreTeam (2019). R: A language and environment for statistical computing. R Foundation for Statistical Computing, Vienna, Austria.
116. Zhu A, Ibrahim JG, and Love MI (2019). Heavy-tailed prior distributions for sequence count data: removing the noise and preserving large differences. Bioinformatics 35, 2084–2092. 10.1093/bioinformatics/bty895. [PubMed: 30395178]
117. Leek JT, Johnson WE, Parker HS, Fertig EJ, Jaffe AE, Zhang Y, Storey JD, and Torres LC (2021). sva: Surrogate Variable Analysis. R package version 3.40.0.
118. Ritchie ME, Phipson B, Wu D, Hu Y, Law CW, Shi W, and Smyth GK (2015). limma powers differential expression analyses for RNA-sequencing and microarray studies. Nucleic Acids Res 43, e47. 10.1093/nar/gkv007. [PubMed: 25605792]
119. Futschik ME, and Carlisle B (2005). Noise-robust soft clustering of gene expression time-course data. J Bioinform Comput Biol 3, 965–988. 10.1142/s0219720005001375. [PubMed: 16078370]
120. Gu Z, Eils R, and Schlesner M (2016). Complex heatmaps reveal patterns and correlations in multidimensional genomic data. Bioinformatics 32, 2847–2849. 10.1093/bioinformatics/btw313. [PubMed: 27207943]
121. Huang da W, Sherman BT, and Lempicki RA (2009). Systematic and integrative analysis of large gene lists using DAVID bioinformatics resources. Nat Protoc 4, 44–57. 10.1038/nprot.2008.211. [PubMed: 19131956]
122. Korotkevich G, Sukhov V, Budin N, Shpak B, Artyomov MN, and Sergushichev A (2021). Fast gene set enrichment analysis. bioRxiv, 060012. 10.1101/060012.
123. Shen L (2021). GeneOverlap: Test and visualize gene overlaps.
124. Corces MR, Trevino AE, Hamilton EG, Greenside PG, Sinnott-Armstrong NA, Vesuna S, Satpathy AT, Rubin AJ, Montine KS, Wu B, et al. (2017). An improved ATAC-seq protocol reduces background and enables interrogation of frozen tissues. Nat Methods 14, 959–962. 10.1038/nmeth.4396. [PubMed: 28846090]
125. Langmead B, and Salzberg SL (2012). Fast gapped-read alignment with Bowtie 2. Nat Methods 9, 357–359. 10.1038/nmeth.1923. [PubMed: 22388286]
126. Zhang Y, Liu T, Meyer CA, Eeckhoute J, Johnson DS, Bernstein BE, Nusbaum C, Myers RM, Brown M, Li W, et al. (2008). Model-based analysis of ChIP-Seq (MACS). Genome Biol 9, R137. 10.1186/gb-2008-9-9-r137. [PubMed: 18798982]
127. Li Q, Brown JB, Huang H, and Bickel PJ (2011). Measuring reproducibility of high-throughput experiments. The Annals of Applied Statistics 5, 1752–1779, 28.
128. Consortium, E.P. (2012). An integrated encyclopedia of DNA elements in the human genome. Nature 489, 57–74. 10.1038/nature11247. [PubMed: 22955616]
129. Liao Y, Smyth GK, and Shi W (2014). featureCounts: an efficient general purpose program for assigning sequence reads to genomic features. Bioinformatics 30, 923–930. 10.1093/bioinformatics/btt656. [PubMed: 24227677]

130. McLean CY, Bristor D, Hiller M, Clarke SL, Schaar BT, Lowe CB, Wenger AM, and Bejerano G (2010). GREAT improves functional interpretation of cis-regulatory regions. Nat Biotechnol 28, 495–501. 10.1038/nbt.1630. [PubMed: 20436461]

131. Ramirez F, Dundar F, Diehl S, Gruning BA, and Manke T (2014). deepTools: a flexible platform for exploring deep-sequencing data. Nucleic Acids Res 42, W187–91. 10.1093/nar/gku365. [PubMed: 24799436]

132. Gu Z, Eils R, Schlesner M, and Ishaque N (2018). EnrichedHeatmap: an R/Bioconductor package for comprehensive visualization of genomic signal associations. BMC Genomics 19, 234. 10.1186/s12864-018-4625-x. [PubMed: 29618320]

133. Kent WJ, Sugnet CW, Furey TS, Roskin KM, Pringle TH, Zahler AM, and Haussler D (2002). The human genome browser at UCSC. Genome Res 12, 996–1006. 10.1101/gr.229102. [PubMed: 12045153]

134. Kaya-Okur HS, Wu SJ, Codomo CA, Pledger ES, Bryson TD, Henikoff JG, Ahmad K, and Henikoff S (2019). CUT&Tag for efficient epigenomic profiling of small samples and single cells. Nat Commun 10, 1930. 10.1038/s41467-019-09982-5. [PubMed: 31036827]

135. Frank SR, Parisi T, Taubert S, Fernandez P, Fuchs M, Chan HM, Livingston DM, and Amati B (2003). MYC recruits the TIP60 histone acetyltransferase complex to chromatin. EMBO Rep 4, 575–580. 10.1038/sj.embor.embor861. [PubMed: 12776177]

136. Quinlan AR, and Hall IM (2010). BEDTools: a flexible suite of utilities for comparing genomic features. Bioinformatics 26, 841–842. 10.1093/bioinformatics/btq033. [PubMed: 20110278]

137. Heinz S, Benner C, Spann N, Bertolino E, Lin YC, Laslo P, Cheng JX, Murre C, Singh H, and Glass CK (2010). Simple combinations of lineage-determining transcription factors prime cis-regulatory elements required for macrophage and B cell identities. Mol Cell 38, 576–589. 10.1016/j.molcel.2010.05.004. [PubMed: 20513432]

138. Ernst J, and Kellis M (2017). Chromatin-state discovery and genome annotation with ChromHMM. Nat Protoc 12, 2478–2492. 10.1038/nprot.2017.124. [PubMed: 29120462]

139. Watanabe K, Taskesen E, van Bochoven A, and Posthuma D (2017). Functional mapping and annotation of genetic associations with FUMA. Nat Commun 8, 1826. 10.1038/s41467-017-01261-5. [PubMed: 29184056]

140. Watanabe K, Umicevic Mirkov M, de Leeuw CA, van den Heuvel MP, and Posthuma D (2019). Genetic mapping of cell type specificity for complex traits. Nat Commun 10, 3222. 10.1038/s41467-019-11181-1. [PubMed: 31324783]

141. Rappsilber J, Ishihama Y, and Mann M (2003). Stop and go extraction tips for matrix-assisted laser desorption/ionization, nanoelectrospray, and LC/MS sample pretreatment in proteomics. Anal Chem 75, 663–670. 10.1021/ac026117i. [PubMed: 12585499]

142. Elias JE, and Gygi SP (2007). Target-decoy search strategy for increased confidence in large-scale protein identifications by mass spectrometry. Nat Methods 4, 207–214. 10.1038/nmeth1019. [PubMed: 17327847]

143. Eng JK, McCormack AL, and Yates JR (1994). An approach to correlate tandem mass spectral data of peptides with amino acid sequences in a protein database. J Am Soc Mass Spectrom 5, 976–989. 10.1016/1044-0305(94)80016-2. [PubMed: 24226387]

144. Kall L, Canterbury JD, Weston J, Noble WS, and MacCoss MJ (2007). Semi-supervised learning for peptide identification from shotgun proteomics datasets. Nat Methods 4, 923–925. 10.1038/nmeth1113. [PubMed: 17952086]

145. Ding S, Mooney N, Li B, Kelly MR, Feng N, Loktev AV, Sen A, Patton JT, Jackson PK, and Greenberg HB (2016). Comparative Proteomics Reveals Strain-Specific beta-TrCP Degradation via Rotavirus NSP1 Hijacking a Host Cullin-3-Rbx1 Complex. PLoS Pathog 12, e1005929. 10.1371/journal.ppat.1005929. [PubMed: 27706223]

146. Bindea G, Mlecnik B, Hackl H, Charoentong P, Tosolini M, Kirilovsky A, Fridman WH, Pages F, Trajanoski Z, and Galon J (2009). ClueGO: a Cytoscape plug-in to decipher functionally grouped gene ontology and pathway annotation networks. Bioinformatics 25, 1091–1093. 10.1093/bioinformatics/btp101. [PubMed: 19237447]

Highlights

- Tip60 acetyltransferase is essential for neuronal specification
- Primary substrate of Tip60 during neuronal induction is histone variant H2A.Z
- Tip60/H2A.Zac promote H3K4me3 deposition and activation of bivalent promoters
- Bivalent gene activation is necessary for neuronal induction

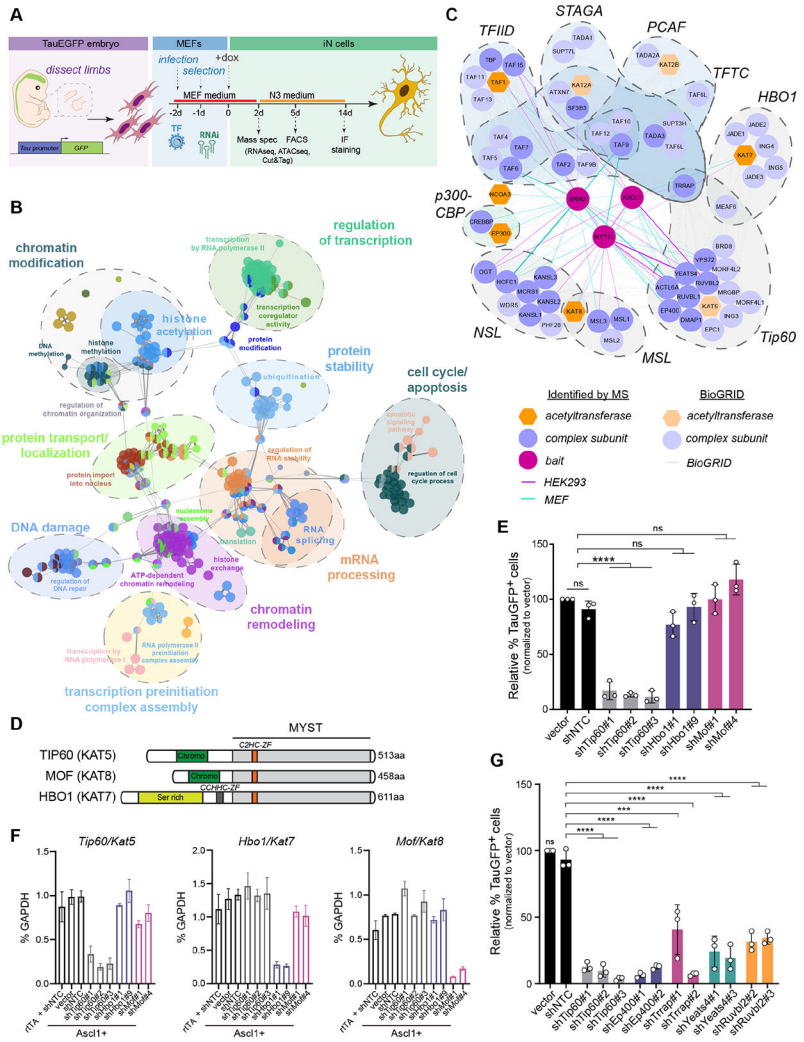

Figure 1. Tip60 interacts with neuronal lineage-determining factors.

(**A**) Design of the study. (**B**) GO enrichment and network analysis of Brn2, Ascl1 and Myt1l interactome. Overrepresented GO Biological Process categories (q-value ≤ 0.05) were clustered into modules and interconnected based on the kappa score (>0.4). Size shows significance, color marks interrelated terms, edge thickness reflects kappa score. (**C**) Subset of PPI network showing interactions of TFs with acetyltransferase complexes. Colored nodes and edges denote candidates identified in this study, translucent nodes and gray edges represent known PPIs (BioGRID). (**D**) MYST acetyltransferases identified in this study. Chromo, chromodomain; C2HC-ZF, C2HC-type zinc finger; Ser-rich, serine-rich; CCHHC-ZF, CCHHC-type zinc finger[93]. (**E**) Fraction of TauGFP^{+} cells at day 5 of reprogramming of TauGFP MEFs transduced with Ascl1 and either vector control, non-targeting control shRNA (shNTC), or shRNAs targeting Tip60, Hbo1 or Mof (n=3). (**F**) qRT-PCR measuring *Tip60*, *Hbo1* and *Mof* transcript levels two days post-Ascl1 induction (n=3; error bars, s.d.). (**G**) TauGFP levels at day 5 of Ascl1 induction (n=3). Statistical significance, (E, G): one-way ANOVA; ****$p<10^{-4}$; ***$p<10^{-3}$; ns, not significant, ($p>0.05$); error bars, s.d.

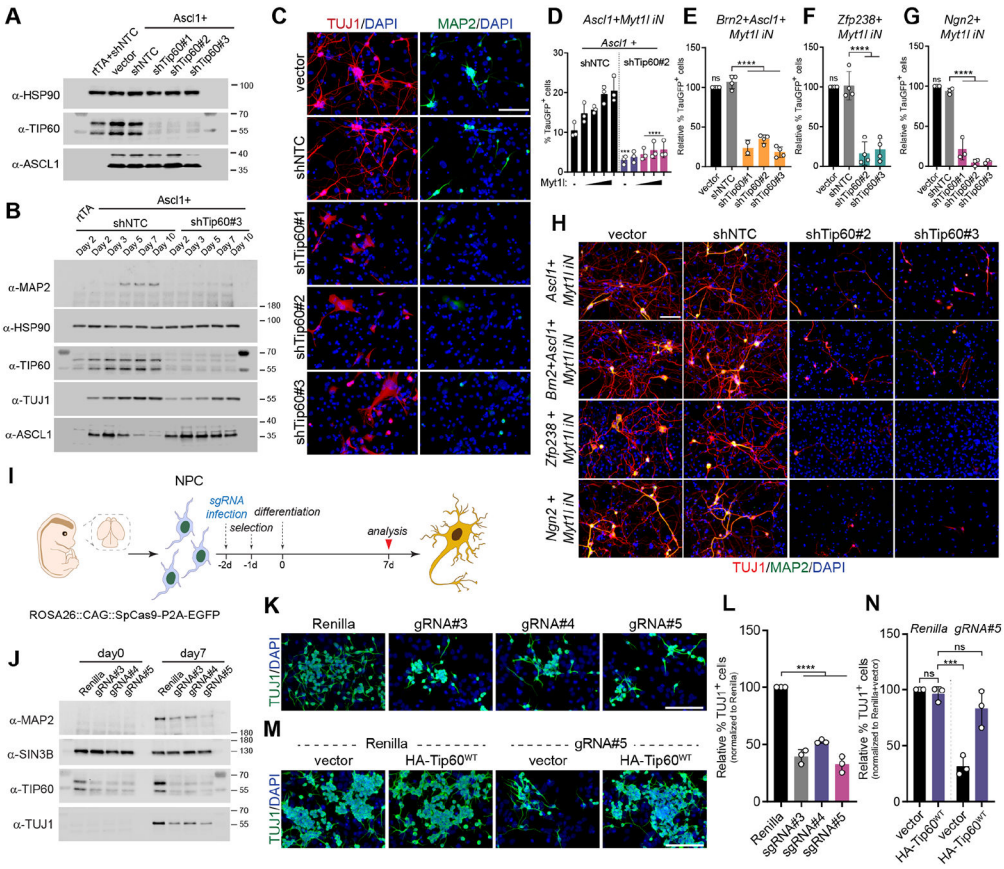

Figure 2. Tip60 is a gate keeper of neuronal cell identity.

(**A** and **B**) Immunoblotting at day 2 (A) or at indicated times (B) of Ascl1 induction in MEFs. (**C**) Representative immunostaining of cells from (A) at day 14. (**D-G**) Absolute (D) or normalized (E-G) TauGFP level at day 5 of reprogramming induced by the combination of the indicated TFs. (**H**) Representative immunostaining of cells from (D-G) at day 14. (**I**) Strategy used to test the effect of Cas9/sgRNA-mediated depletion of Tip60 on NPCs differentiation. (**J**) Immunoblotting at days 0 and 7 of the differentiation of NPCs expressing sgRNA control (Renilla) or Tip60 sgRNAs (sgRNA#3-#5). (**K** and **L**) Differentiation of NPCs assessed at day 7 by anti-TUJ1 immunostaining. Shown are (K) representative immunostaining and (L) differentiation efficiency as a fraction of TUJ^+ cells (n=3). (**M** and **N**) NPCs were co-infected with sgRNAs and a vector control or HA-$Tip60^{WT}$. Shown are (M) representative immunostaining and (N) differentiation efficiency determined as in (L) (n=3). Statistical significance, (D-G, L, N): one way ANOVA; ****$p<10^{-4}$; ***$p<10^{-3}$; ns, not significant ($p>0.05$); error bars, s.d. Scale bars: 100μm.

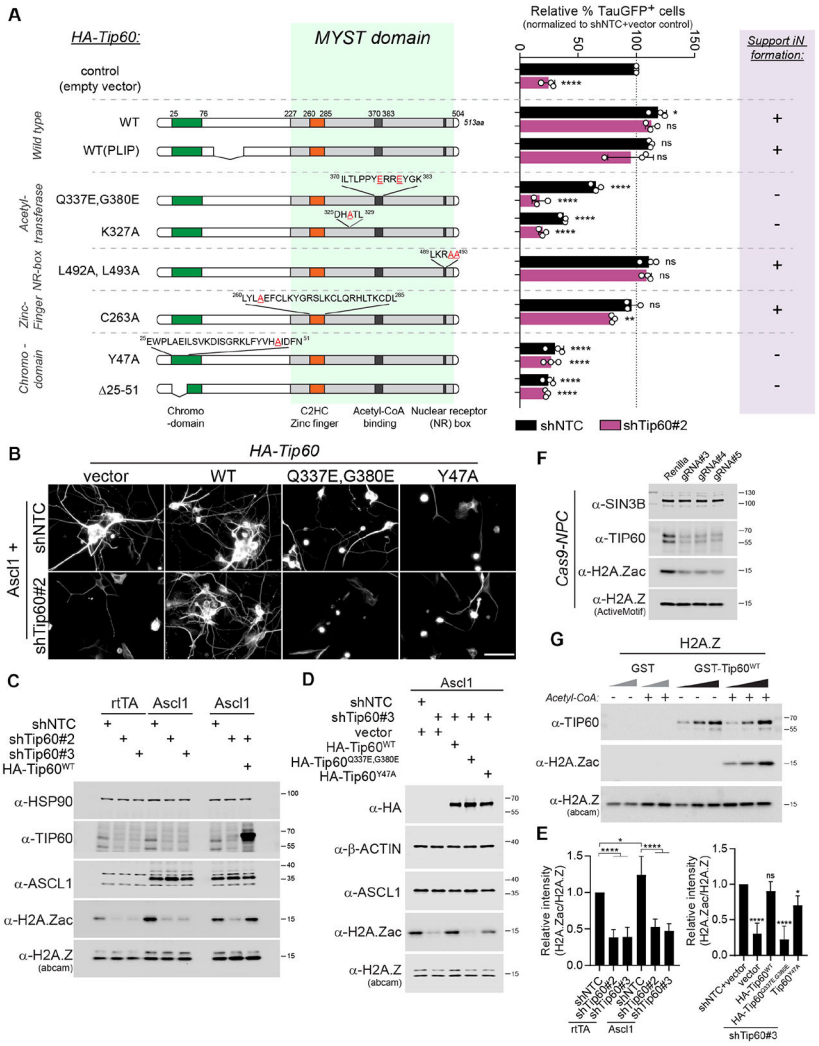

Figure 3. Tip60 acetylates H2A.Z during neuronal induction.

(**A**) Effect of point and Tip60 truncation mutant proteins on the induction of TauGFP by Ascl1. (Left) Constructs used in structure-function analysis. Point mutations are highlighted in red. PLIP, a splice variant of Tip60. (Right) Fraction of TauGFP^{+} cells at day 5 of Ascl1 induction in presence of shNTC (black) or shTip60#2 (purple), and either vector control or indicated Tip60 constructs. (**B**) Representative immunostaining of selected conditions from (A) at day 14 (see also Figure S4C). Scale bar: 50μm. (**C-F**) Immunoblotting of total MEF lysates at day 2 post-dox (C and D) or NPCs lysates at day 4 post-infection (F). (E) Quantification of H2A.Zac signals from (C) (left, n=5) and (E) (right, n=4). (**G**) *In vitro* acetylation of recombinant H2A.Z using purified GST-Tip60, or GST alone, in the presence or absence of acetyl-CoA. Statistical significance, (A, E): one way ANOVA; ****$p<10^{-4}$; **$p<10^{-2}$; *$p<0.05$; ns, not significant, ($p>0.05$); error bars, s.d.

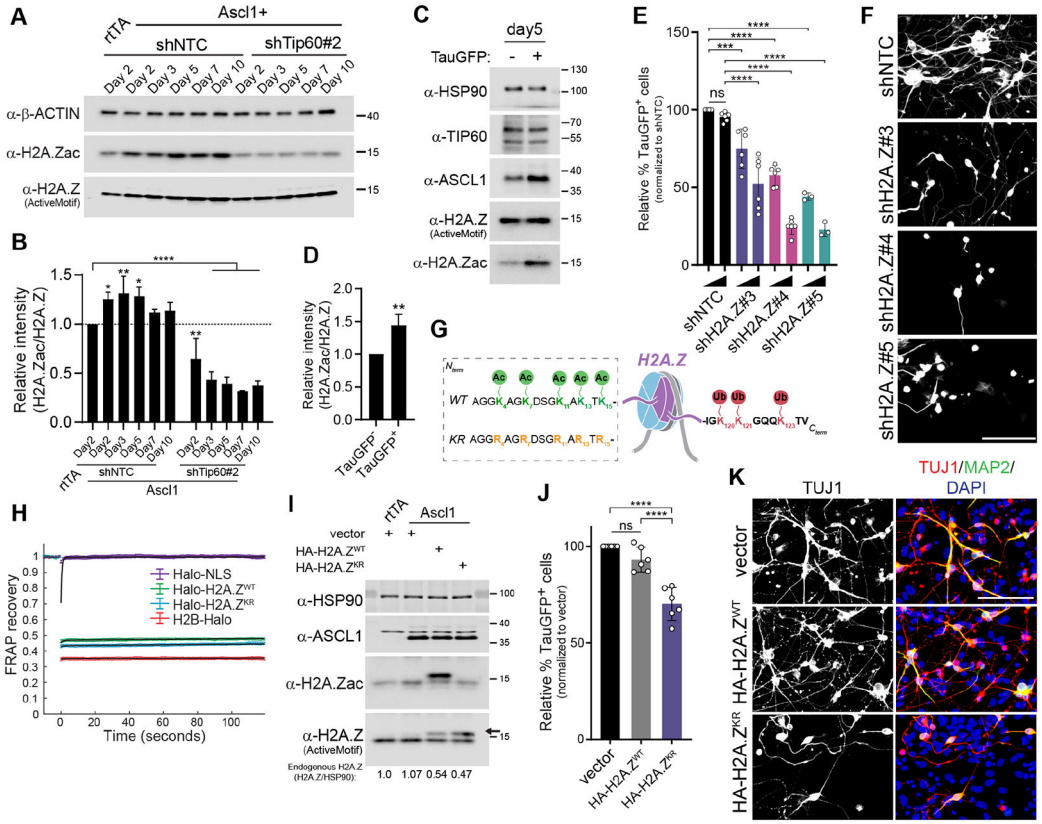

Figure 4. H2A.Z acetylation is critical for neuronal specification.

(**A** and **B**) Immunoblotting (A) and the quantified H2A.Zac intensity (B) at indicated times of Ascl1 induction. (**C** and **D**) Comparison of immunoblotting signals (C) and normalized H2A.Zac levels (D) in TauGFP^{+} and TauGFP^{-} Ascl1-iN cells. (**E**) Fraction of TauGFP^{+} cells at day 5 of Ascl1-induced reprogramming in the presence of increasing amounts of control or shH2A.Z (n≥3). (**F**) Representative immunostaining of cells from (E) at day 14. (**G**) Schematics of H2A.Z N- and C-terminal amino acid sequences showing acetylation (Ac) and ubiquitination (Ub) sites, and lysines that were mutated to generate acetylation-resistant H2A.Z^{KR}. (**H**) FRAP analysis of Halo-tagged H2A.Z^{WT}, H2A.Z^{KR}, H2B, or Halo-NLS. Fluorescence intensity recovery was measured at the bleach spot in MEFs labeled with HaloLigand-JF549, at day 2 (n=21 cells, 3 biological replicates; error bars, s.e.m; NLS, nuclear localization signal). (**I**) Immunoblotting at day 2 of Ascl1 induction. Quantification of endogenous H2A.Z, normalized to HSP90 and to the vector control is shown below. (**J** and **K**) H2A.Zac is required for neuronal induction. Fraction of TauGFP^{+} cells at day 5 (n=6) (J) and representative immunostaining of the quantified cells at day 14 (K) (see also Figure S5L). Statistical significance, (D): unpaired two-tailed Student's t-test; (B, E and J): one way ANOVA; ****$p<10^{-4}$; **$p<10^{-2}$; *$p<0.05$; ns, not significant, ($p>0.05$); error bars, s.d. Scale bars: 100μm.

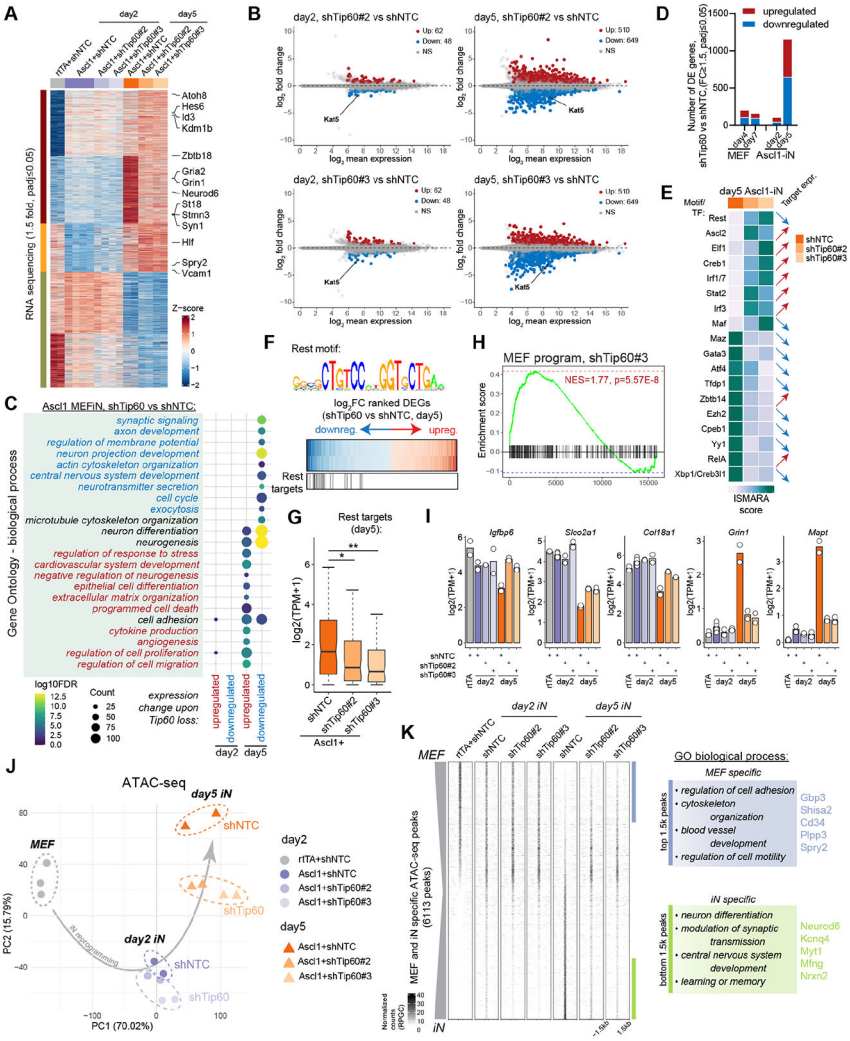

Figure 5. Tip60 is required for suppression of fibroblast cell identity and induction of neuronal fate.

(**A**) Fuzzy c-means clustering of differentially expressed genes (DEGs) identified by RNA-seq at days 2 and 5 of Ascl1 induction (n=2, biological replicates; 4,215 DEGs, fold change (fc)≥1.5, padj≤0.05). (**B**) MA plots of pairwise DE analyses between control and shTip60-expressing Ascl1-iN cells at day 2 (left) or day 5 (right). Upregulated (Up) and downregulated (Down) genes are colored in red and blue, respectively. NS; not significant. (**C**) GO Biological Process term enrichment analysis of genes upregulated (red) or downregulated (blue) upon Tip60 RNAi in Ascl1-iNs. (**D**) Number of DEGs detected upon Tip60 RNAi in MEFs or Ascl1-iNs. X-axis shows days post-infection (MEF) or post-induction (Ascl1-iN). (**E**) ISMARA and predicted TF activity in day 5 Ascl1-iNs. Arrows indicate TF target gene expression (relative to shNTC control): upregulated, red; downregulated, blue. Elevated E-box motif activity likely results from a higher Ascl1 expression in Tip60-depleted cells. (**F** and **G**) Impaired expression of Rest targets in shTip60 cells. (F) Day 5 DEGs ranked based on log_2fc, with upregulated and downregulated genes labeled in red and blue, respectively. Position of Rest targets is indicated below. (G) Expression of Rest targets in day 5 Ascl1-iNs (Wilcoxon test, unpaired; ****$padj$<10^{-4};

$padj$<0.01; *$padj$<0.05). (H**) GSEA of MEF signature in day 5 DEGs (Ascl1+shNTC vs Ascl+shTip60#3). NES, normalized enrichment score. (**I**) Expression of selected fibroblast and neuronal genes (n=2, RNAseq). (**J**) PCA of ATAC-seq datasets (n=2, biological replicates). (**K**) Tip60 knockdown interferes with chromatin "switch" associated with iN reprogramming. Average normalized ATAC-seq read count within ±1.5kb of MEF- and iN-specific open chromatin sites that changed accessibility upon Tip60 RNAi by day 5 (6113 sites, fc≥2, padj≤0.05, with respect to shNTC). Heatmap was sorted based on the fc enrichment between day 5 Ascl1+shNTC and rtTA+shNTC. GO term enrichment of the top 1.5k MEF- and iN-specific sites, and selected genes contributing to the terms (right).

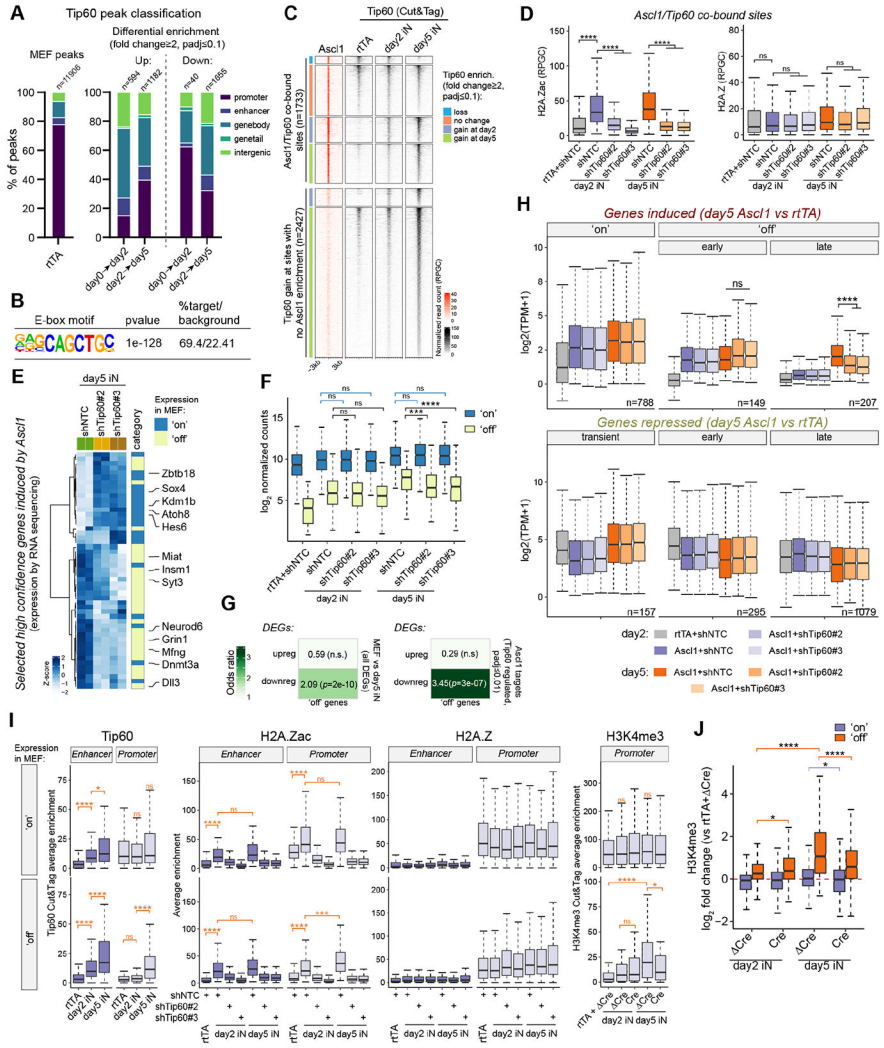

Figure 6. Tip60 promotes H3K4me3 deposition and silent gene activation.

(**A**) Classification of Tip60 peaks in MEFs (left) and Tip60 peaks that are differentially enriched between MEFs and day 2 Ascl1-iN (day0-day2), or day 2 Ascl1-iN and day 5 TauGFP^{+} Ascl1-iN (day2-day5), (fc≥2, padj≤0.1). Shown are peaks that gain (Up) or lose (Down) enrichment. (**B**) E-box motif enrichment at sites gaining Tip60 at day 2. (**C**) Dynamics of Tip60 binding at Ascl1/Tip60 co-occupied sites (top) and at sites gaining Tip60 in the absence of Ascl1 binding (bottom). (**D**) Normalized (RPGC) H2A.Zac (left) or H2A.Z (right) read counts at Ascl1/Tip60 co-bound sites (Ascl1 peak summit±250bp). (**E-G**) Tip60 depletion affects induction of silent (‘off’) genes by Ascl1. (E) Day 5 expression of selected Ascl1 targets (blue, left) and their corresponding ‘on’ (active) and ‘off’ (silent) expression category (right) (see also Methods). (F) Expression of all ‘on’/ ‘off’ Tip60-regulated Ascl1 targets (padj≤0.01). (G) Association between the direction of the expression change determined for the ‘off’ genes identified among the indicated groups of DEGs. Numbers show Odds ratio; *p* values are in brackets; n.s., not significant. (**H**) Expression of genes induced (top) or repressed (bottom) during 5 days of neuronal induction. (**I**) Normalized read count (RPGC) at the ‘on’ (top) and ‘off’ (bottom) Ascl1

target gene enhancers and promoters was determined for Tip60, H2A.Zac and H2A.Z in TauGFP MEFs (Ascl1 peak summit or TSS, ±250bp), and for H3K4me3 (TSS±500bp) in Cre/ΔCre-transduced Tip60 cKO MEFs. (**J**) $\log_2$ fc in H3K4me3 read count (RPGC, TSS±500bp), with respect to rtTA+ΔCre, was determined for the 'on'/'off' genes during Tip60 cKO MEF reprogramming. The values were plotted for day 5 DEGs (MEF vs day5 Ascl1-iN, fc≥1.5, padj≤0.05) that were significantly affected by Tip60 depletion. Statistical significance: (D, F, H-J) unpaired Wilcoxon test; ****$padj<10^{-4}$; ***$padj<10^{-3}$; *$padj<0.05$; ns, not significant.

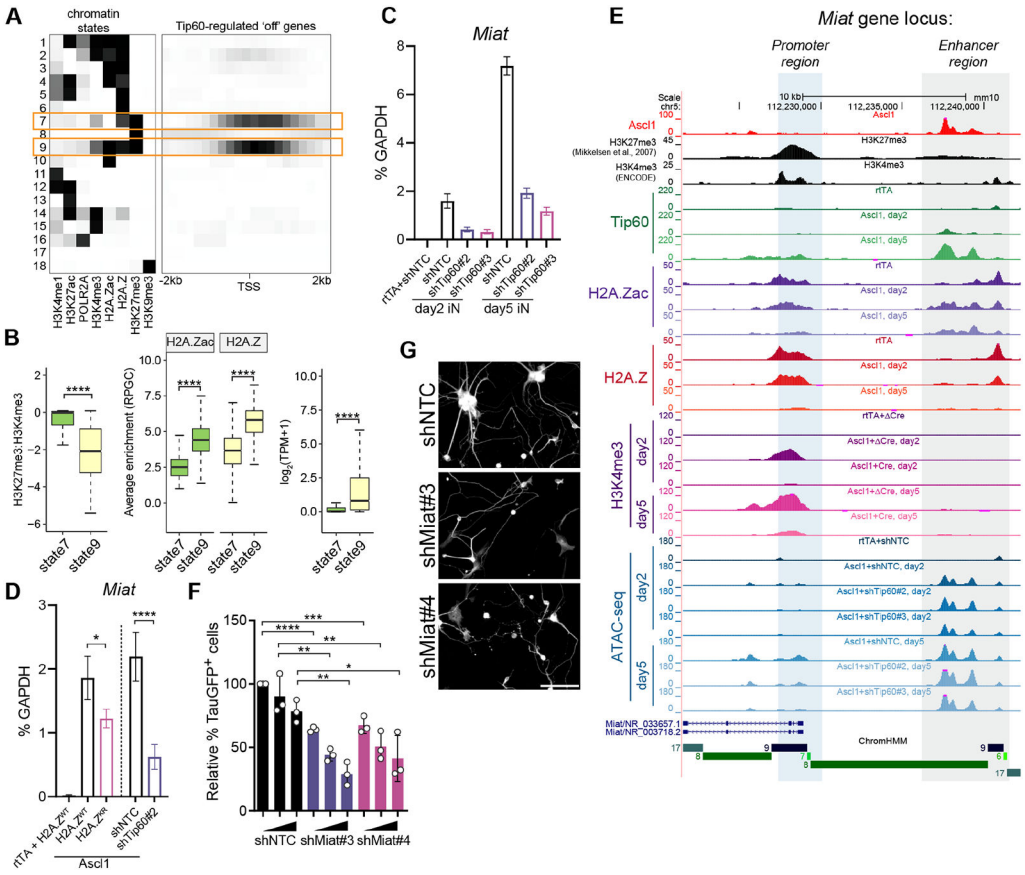

Figure 7. Tip60/H2A.Zac promote activation of bivalent genes critical for neuronal induction.

(**A**) Chromatin states (left) and chromatin state enrichment within TSS±2kb of Tip60-regulated 'off' genes (right) determined by ChromHMM. (**B**) Normalized H3K27me3 and H3K4me3 (TSS±500bp), and H2A.Zac and H2A.Z (TSS±250bp) read counts were determined for MEF genes with TSS overlapping ChromHMM states. Shown are: H3K27me3:H3K4me3 ratio (left), H2A.Zac and H2A.Z enrichment (middle), and average gene expression (right). (**C** and **D**) qRT-PCR measuring *Miat* levels in control and Ascl1-iN cells at indicated times (C) (n=3; error bars, s.e.m.), or at day 2 of neuronal induction (D) (n=5; error bars s.d.). (**E**) ChIP-seq (Ascl1, H3K27me3, H3K4me3(ENCODE)), Cut&Tag (Tip60, H2A.Zac, H2A.Z, H3K4me3) and ATAC-seq signal tracks showing chromatin dynamics at *Miat* gene locus in MEFs (black) and during neuronal reprogramming. ChromHMM chromatin states defined in (A) are depicted below. Promoter-proximal region (blue) and enhancer region (gray) are shown. (**F-G**) Fraction of TauGFP^{+} cells at day 5 (n=3; error bars, s.d.) (F), and representative immunostaining at day 14 (G) of Ascl1-induced reprogramming. Statistical significance, (B): unpaired Wilcoxon test; (D, F): one-way ANOVA. ****$p<10^{-4}$; ***$p<10^{-3}$; **$p<10^{-2}$; *$p<0.05$; ns, not significant ($p>0.05$). Scale bar: 100μm.

KEY RESOURCES TABLE

REAGENT or RESOURCE	SOURCE	IDENTIFIER
Antibodies		
MAP2	Abcam	Cat# ab5392; RRID:AB_2138153
MAP2	Sigma-Aldrich	Cat# M9942; RRID:AB_477256
TUJ1	BioLegend	Cat# 801202; RRID:AB 10063408
HA.11 (mouse)	BioLegend	Cat# 901501; RRID:AB_2565006
HA.11 (rabbit)	BioLegend	Cat# 902301; RRID:AB_2565018
H2A.Zac (Lys4/Lys7)	Cell Signaling Technology	Cat# 75336; RRID:AB_2799867
Ki67	BD Biosciences	Cat# 550609; RRID:AB_393778
HSP90	Cell Signaling Technology	Cat# 4874; RRID:AB_2121214
TIP60	Santa Cruz Biotechnology	Cat# sc-166323; RRID:AB_2296327
TIP60	Frank et al., 2003[135]	gift from Dr. Bruno Amati
ASCL1	Abcam	Cat# ab74065; RRID:AB_1859937
FLAG	Sigma-Aldrich	Cat# F7425; RRID:AB_439687
SIN3B	Santa Cruz Biotechnology	Cat# sc-996; RRID:AB_2187785
β-ACTIN	Sigma-Aldrich	Cat# A5441; RRID:AB_476744
DESMIN	Abcam	Cat# ab32362; RRID:AB_731901
H2Aac	Cell Signaling Technology	Cat# 2576; RRID:AB_2118805
H2A	Cell Signaling Technology	Cat# 12349; RRID:AB_2687875
H2A.Z	Active Motif	Cat# 39113; RRID:AB_2615081
H2A.Z	Abcam	Cat# ab4174; RRID:AB_304345
H3K9ac	Cell Signaling Technology	Cat# 9649; RRID:AB_823528
H3K14ac	Cell Signaling Technology	Cat# 7627; RRID:AB_10839410
H3K18ac	Cell Signaling Technology	Cat# 13998; RRID:AB_2783723
H3K27ac	Abcam	Cat# ab4729; RRID:AB_2118291
H3K56ac	Cell Signaling Technology	Cat# 4243; RRID:AB_10548193
H3	Cell Signaling Technology	Cat# 3638; RRID:AB_1642229
H4K5ac	Cell Signaling Technology	Cat# 8647; RRID:AB_11217428
H4K12ac	Cell Signaling Technology	Cat# 13944; RRID:AB_2798350
H4K16ac	Millipore	Cat# 07-329; RRID:AB_310525
H4	Cell Signaling Technology	Cat# 2935; RRID:AB_1147658
H3K4me3	Active Motif	Cat# 39159; RRID:AB_2615077
APC-BrdU (3D4)	BioLegend	Cat# 364114; RRID:AB_2814315
FLAG M2 affinity agarose	Sigma-Aldrich	Cat# A2220; RRID:AB_10063035
Pierce™ Anti-HA Magnetic Beads	Thermo Fisher Scientific	Cat# 88836; RRID:AB_2861399
guinea pig anti-rabbit IgG	antibodies online	Cat# ABIN101961; RRID:AB_10775589
Bacterial and virus strains		
E. coli: T7 Express lysY/Iq	New England Biolabs	Cat# C3013I

REAGENT or RESOURCE	SOURCE	IDENTIFIER
E. coli: BL21(DE3)	Agilent	Cat# 200131
Chemicals, peptides, and recombinant proteins		
DMEM media	Gibco	Cat# 11965-092
DMEM/F12 media	Gibco	Cat# 11320-033
N2 supplement	Gibco	Cat# 17502-048
B27 supplement	Gibco	Cat# 17504-044
Insulin	Sigma-Aldrich	Cat# I6634
FGF	PeproTech	Cat# PHG0263
EGF	R&D Systems	Cat# 236-EG-01M
KnockOut™ Serum	Thermo Fisher Scientific	Cat# 10828-028
HyClone™ Fetal Bovine Serum	Thermo Fisher Scientific	Cat# SH30071.03
HyClone™ Cosmic Calf Serum	Thermo Fisher Scientific	Cat# SH30087.04
Horse Serum	Thermo Fisher Scientific	Cat# 26050-070
SpCas9	Integrated DNA Technologies	Cat# 1081058
Opti-MEM™	Thermo Fisher Scientific	Cat# 31985-062
Polyethyleneimine (PEI)	Polysciences Inc.	Cat# 23966-2
Accutase	Thermo Scientific	Cat# NC9464543
Doxycycline	Sigma-Aldrich	Cat# P3655
SU9516	Selleckchem	Cat# S7636
Shield-1	Cheminpharma	Cat# S1-0001
APC Annexin V	BD Biosciences	Cat# 550475
5-Bromo-2′-deoxyuridine	Sigma-Aldrich	Cat# B5002
JF-549-HaloTagLigand	Grimm et al., 2015[110]	gift from Dr Luke Lavis
cOmplete™, EDTA-free Protease Inhibitors	Roche	Cat# 11873580001
FLAG peptide	Sigma-Aldrich	Cat# F3290
Digitonin	Millipore	Cat# 300410
Proteinase K	Thermo Fisher Scientific	Cat# ABIN101961
Benzonase	Millipore	Cat# 1016540001
Dithiothreitol	Promega	Cat# V3151
Iodoacetamide	Sigma-Aldrich	Cat# I1149
Sequencing Grade Modified Trypsin	Promega	Cat# V5113
TRIzol	Invitrogen	Cat# 15596026
SYBR green	Applied Biosystems	Cat # 4367659
Acetyl-CoA	Sigma-Aldrich	Cat# A2056
MNase	Thermo Fisher Scientific	Cat# 88216
AMPure XP	Beckman Coulter	Cat# A63881
RQ1 RNAse-free DNAse	Promega	Cat# M6101
Concanavalin A beads	Bangs Laboratories	Cat# BP531
Dynabeads™ MyOne™ Streptavidin C1	Thermo Fisher Scientific	Cat# 65001

REAGENT or RESOURCE	SOURCE	IDENTIFIER
Ni-nitrilotriacetic acid (NTA) resin	Qiagen	Cat# 30210
Novagen™ S-protein Agarose	Sigma-Aldrich	Cat# 697043
Glutathione Sepharose 4b	GE Healthcare	Cat# 17-0756-01
Recombinant histone H2A.Z	Millipore	Cat# 14-1109
Critical commercial assays		
mES Cell Nucleofector® Kit	Lonza	Cat# VAPH-1001
Ovation RNA-seq System V2	NuGEN	Cat# 7102-08
NEBNext Ultra DNA Library Prep Kit	New England Biolabs	Cat# E7370S
NEB Next High-Fidelity 2x PCR Master Mix	New England Biolabs	Cat# M0541L
SuperScript™ III First-Strand Synthesis System	Thermo Fisher Scientific	Cat# 18080-051
Deposited data		
RNA-seq	This paper	GEO: GSE181965
ATAC-seq	This paper	GEO: GSE181965
Cut&Tag	This paper	GEO: GSE181965
MEF: H3K4me1 ChIP-seq	ENCODE	ENCSR000CAZ
MEF: H3K4me3 ChIP-seq	ENCODE	ENCSR000CBA
MEF: CTCF ChIP-seq	ENCODE	ENCSR000CBW
MEF: POLR2A ChIP-seq	ENCODE	ENCSR000CBX
MEF: H3K27ac ChIP-seq	ENCODE	ENCSR000CDI
MEF: Control ChIP-seq	ENCODE	ENCSR000CBB
MEF: H3K27me3, H3K36me3, H3K9me3 ChIP-seq	Mikkelsen et al., 2007[69]	GEO: GSE12241
MEFiN ATAC-seq and RNA-seq	Wapinski et al., 2017[16]	GEO: GSE101397
Ascl1 ChIP-seq	Wapinski et al., 2013[17]	GEO: GSE43916
Experimental models: Cell lines		
v6.5	Rideout et al., 2000[95]	RRID:CVCL_C865
v6.5-TetO-Ascl1	This paper	N/A
Flp-In T-Rex™ HEK293	Thermo Fisher Scientific	Cat#R78007
HEK293T	ATCC	Cat#11268
Experimental models: Organisms/strains		
Mouse: Crl:CD1(ICR)	Charles River	RRID:IMSR_CRL:022
Mouse: DR4	Jackson Laboratory	RRID:IMSR_JAX:003208
Mouse: C57BL/6J	Jackson Laboratory	RRID:IMSR_JAX:000664
Mouse: Gt(ROSA)26Sor$^{tm1.1(CAG-cas9*,-EGFP)Fezh}$/J	Jackson Laboratory	RRID:IMSR_JAX:024858
Mouse: Mapt$^{tm1(EGFP)Klt}$/J	Jackson Laboratory	RRID:IMSR_JAX:004779
Mouse: Kat5fl/fl	This paper	N/A
Oligonucleotides		
See Table S6	N/A	N/A
Recombinant DNA		
FUW-TetO-Ascl1	Vierbuchen et al., 2010[15]	RRID:Addgene_27150

REAGENT or RESOURCE	SOURCE	IDENTIFIER
FUW-TetO-Brn2	Vierbuchen et al., 2010[15]	RRID:Addgene_27151
FUW-TetO-Myt1l	Vierbuchen et al., 2010[15]	RRID:Addgene_27152
FUW-TetO-Ngn2-puro	Zhang et al., 2013[49]	RRID:Addgene_52047
FUW-TetO-Zfp238	Wapinski et al., 2017[16]	N/A
FUW-TetO-FLAG-MyoD1	Lee et al., 2020[98]	N/A
FUW-TetO-FLAG/His^{7}-Ascl1	This paper	N/A
FUW-TetO-FLAG/His^{7}-Myt1l$^{200–623}$	This paper	N/A
FUW-TetO-BirA-Ascl1	This paper	N/A
FUW-TetO-BirA-Brn2	This paper	N/A
FUW-TetO-BirA-Myt1l$^{200–623}$	This paper	N/A
FUW-M2rtTA	Hockemeyer et al., 2008[107]	RRID:Addgene_20342
pG-LAP6-Ascl1	This paper	N/A
pG-LAP7-Ascl1	This paper	N/A
pG-LAP6-Brn2	This paper	N/A
pG-LAP6- Myt1l$^{200–623}$	This paper	N/A
pG-LAP6- Myt1l	This paper	N/A
FUW-TetO-HA-TIP60	This paper	N/A
FUW-TetO-HA-TIP60(PLIP)	This paper	N/A
FUW-TetO-HA-TIP60(Q337E/G380E)	This paper	N/A
FUW-TetO-HA-TIP60(K327A)	This paper	N/A
FUW-TetO-HA-TIP60(L492A/L493A)	This paper	N/A
FUW-TetO-HA-TIP60(C263A)	This paper	N/A
FUW-TetO-HA-TIP60(Y47A)	This paper	N/A
FUW-TetO-HA-TIP60(Δ25-51)	This paper	N/A
DD-Cas9-P2A-Puro (pEDCPP)	This paper	N/A
pEDCPP-Renilla	This paper	N/A
pEDCPP-Tip60-gRNA#3	This paper	N/A
pEDCPP-Tip60-gRNA#4	This paper	N/A
pEDCPP-Tip60-gRNA#5	This paper	N/A
pSico-Puro	N/A	gift from Tyler Jacks
pSico-Puro-shNTC	This paper	N/A
pSico-Puro-shTip60#1	This paper	N/A
pSico-Puro-shTip60#2	This paper	N/A
pSico-Puro-shTip60#3	This paper	N/A
pSico-Puro-shHbo#1	This paper	N/A
pSico-Puro-shHbo#9	This paper	N/A
pSico-Puro-shMof#1	This paper	N/A
pSico-Puro-shMof#4	This paper	N/A
pSico-Puro-shEp400#1	This paper	N/A

REAGENT or RESOURCE	SOURCE	IDENTIFIER
pSico-Puro-shEp400#2	This paper	N/A
pSico-Puro-shTrrap#1	This paper	N/A
pSico-Puro-shTrrap#2	This paper	N/A
pSico-Puro-shYeats#1	This paper	N/A
pSico-Puro-shYeats#3	This paper	N/A
pSico-Puro-shRuvbl#2	This paper	N/A
pSico-Puro-shRuvbl#3	This paper	N/A
pSico-Puro-shH2A.Z.1#3	This paper	N/A
pSico-Puro-shH2A.Z.1#4	This paper	N/A
pSico-Puro-shH2A.Z.1#5	This paper	N/A
pLentiGuide	Rubin et al., 2019[99]	RRID:Addgene_117986
pLentiGuide-Renilla	This paper	N/A
pLentiGuide-Tip60-gRNA#3	This paper	N/A
pLentiGuide-Tip60-gRNA#4	This paper	N/A
pLentiGuide-Tip60-gRNA#5	This paper	N/A
FUW-TetO-H2A.Z.1^{WT}-HA	This paper	N/A
FUW-TetO-H2A.Z.1^{KR}-HA	This paper	N/A
FUW-TetO-Halo-NLS	This paper	N/A
FUW-TetO-Halo- H2A.Z.1^{WT}	This paper	N/A
FUW-TetO-Halo- H2A.Z.1^{KR}	This paper	N/A
FUW-TetO-H2B-Halo	This paper	N/A
FUW-NLS-EGFP-Cre	This paper	N/A
FUW-NLS-EGFP-ΔCre	This paper	N/A
PiggyBac-TetO-Ascl1-neomycin	Ng et al., 2021[96]	RRID:Addgene_176482
pOG44	Invitrogen	Cat# V6005-20
3XFlag-pA-Tn5-Fl	Kaya-Okur et al., 2019[134]	RRID:Addgene_124601
pGEX6P1-TIP60	This paper	N/A
Software and algorithms		
MatLab	The Mathworks, Inc.	RRID:SCR_001622; https://www.mathworks.com/products/matlab.html
Prism	GraphPad	RRID:SCR_002798; http://www.graphpad.com/
R	R Core Team, 2019[115]	https://www.r-project.org/
skewer (v0.2.2)	Jiang et al., 2014[112]	RRID:SCR_001151; https://sourceforge.net/projects/skewer
salmon (v1.4.0)	Patro et al., 2017[113]	RRID:SCR_017036; https://combine-lab.github.io/salmon/
DESeq2	Love et al., 2014[114]	RRID:SCR_015687; https://bioconductor.org/packages/DESeq2/
Apeglm	Zhu et al., 2019[116]	https://github.com/azhu513/apeglm

REAGENT or RESOURCE	SOURCE	IDENTIFIER
sva	Leek et al., 2021[117]	RRID:SCR_012836; https://bioconductor.org/packages/sva/
limma	Ritchie et al., 2015[118]	RRID:SCR_010943; https://bioconductor.org/packages/limma/
Mfuzz (v2.44.0)	Futschik and Carlisle, 2005[119]	RRID:SCR_000523; https://bioconductor.org/packages/Mfuzz/
DAVID 6.8	Huang da et al., 2009[121]	RRID:SCR_001881; https://david.ncifcrf.gov/
fgsea	Korotkevich et al., 2021[122]	RRID:SCR_020938; https://bioconductor.org/packages/fgsea/
ISMARA	Balwierz et al., 2014[65]	https://ismara.unibas.ch/mara/
GeneOverlap (v1.28.0)	Shen, 2021[123]	RRID:SCR_018419; https://bioconductor.org/packages/GeneOverlap/
cutadapt	N/A	RRID:SCR_011841; https://cutadapt.readthedocs.io/en/stable/
Bowtie2	Langmead and Salzberg, 2012[125]	RRID:SCR_016368; http://bowtie-bio.sourceforge.net/bowtie2/index.shtml
MACS2 (v2.2.7.1)	Zhang et al., 2008[125]	RRID:SCR_013291; https://github.com/macs3-project/MACS
IDR	Li et al., 2011[127]	RRID:SCR_017237; https://github.com/nboley/idr
ENCODE ATAC-seq pipeline v1.2.0	Consortium, 2012[128]	https://github.com/ENCODE-DCC/atac-seq-pipeline
featureCounts	Liao et al., 2014[129]	RRID:SCR_012919; http://subread.sourceforge.net/
BEDTools	Quinlan and Hall, 2010[136]	RRID:SCR_006646; https://github.com/arq5x/bedtools2
GREAT	McLean et al., 2010[130]	RRID:SCR_005807; http://great.stanford.edu/public/html/splash.php
deepTools	Ramirez et al., 2014[131]	RRID:SCR_016366; https://deeptools.readthedocs.io/en/develop/
HOMER (v4.11.1)	Heinz et al., 2010[137]	RRID:SCR_010881; http://homer.ucsd.edu/homer/
ChromHMM (v1.20)	Ernst and Kellis, 2017[138]	RRID:SCR_018141; http://compbio.mit.edu/ChromHMM/
Functional Mapping and Annotation (FUMA)	Watanabe et al., 2017[139] Watanabe et al., 2019[140]	RRID:SCR_017521; https://fuma.ctglab.nl/
UCSC genome browser	Kent et al., 2002[133]	RRID:SCR_005780; http://genome.ucsc.edu/
Cytoscape	Shannon et al., 2003[39]	RRID:SCR_003032; http://cytoscape.org
ClueGO	Bindea et al., 2009[146]	RRID:SCR_005748; http://www.ici.upmc.fr/cluego/
Adobe Illustrator	Adobe	RRID:SCR_010279; http://www.adobe.com/products/illustrator.html
Fiji/ImageJ	Schindelin et al., 2012[108]	RRID:SCR_002285; http://fiji.sc
Image Studio Lite	LI-COR	RRID:SCR_013715; https://www.licor.com/bio/image-studio-lite/
Image Lab	BioRad	RRID:SCR_014210; http://www.bio-rad.com

REAGENT or RESOURCE	SOURCE	IDENTIFIER
FlowJo	BD Biosciences	RRID:SCR_008520; https://www.flowjo.com/solutions/flowjo
Other		
BioGRID database	Oughtred et al., 2019[38]	RRID:SCR_007393; http://www.thebiogrid.org/